



Transmembrane Helix Integrity versus Fraying to

Article

Expose Hydrogen Bonds at a Membrane-Water Interface

Fahmida Afrose, Matthew J. McKay, Armin Mortazavi, Vasupradha Suresh Kumar, Denise V. Greathouse, and Roger E. Koeppe *Biochemistry*, **Just Accepted Manuscript •** DOI: 10.1021/acs.biochem.8b01119 • Publication Date (Web): 19 Dec 2018 **Downloaded from http://pubs.acs.org on December 19, 2018**

Just Accepted

"Just Accepted" manuscripts have been peer-reviewed and accepted for publication. They are posted online prior to technical editing, formatting for publication and author proofing. The American Chemical Society provides "Just Accepted" as a service to the research community to expedite the dissemination of scientific material as soon as possible after acceptance. "Just Accepted" manuscripts appear in full in PDF format accompanied by an HTML abstract. "Just Accepted" manuscripts have been fully peer reviewed, but should not be considered the official version of record. They are citable by the Digital Object Identifier (DOI®). "Just Accepted" is an optional service offered to authors. Therefore, the "Just Accepted" Web site may not include all articles that will be published in the journal. After a manuscript is technically edited and formatted, it will be removed from the "Just Accepted" Web site and published as an ASAP article. Note that technical editing may introduce minor changes to the manuscript text and/or graphics which could affect content, and all legal disclaimers and ethical guidelines that apply to the journal pertain. ACS cannot be held responsible for errors or consequences arising from the use of information contained in these "Just Accepted" manuscripts.



Transmembrane Helix Integrity versus Fraying to Expose Hydrogen Bonds at a Membrane-Water Interface

Fahmida Afrose, Matthew J. McKay, Armin Mortazavi, Vasupradha Suresh Kumar, Denise V. Greathouse, Roger E. Koeppe II*

Department of Chemistry and Biochemistry, University of Arkansas, Fayetteville, Arkansas 72701, United States KEYWORDS: Solid-state deuterium NMR, transmembrane helix fraying, histidine, tryptophan, membrane protein.

1 ABSTRACT: Transmembrane helices dominate the landscape for many membrane proteins. Often flanked by interfacial aromatic residues, these transmembrane helices also contain loops and inter-helix segments, which could help in stabilizing a transmembrane orientation. Using ²H-NMR spectroscopy to monitor bilayer incorporated model GWALP23 family peptides, we address systematically the issue of helix fraying in relation to the dynamics and orientation of closely similar individual transmembrane helices. Adjacent to a core transmembrane helix, we inserted aromatic (Phe, Trp, Tyr, His) or non-aromatic residues (Ala, Gly) into positions 4 and 5, to examine the side-chain dependency of the transmembrane orientation, dynamics and helix integrity (extent and location of unraveling). Incorporation of ²H-alanine labels enables one to assess the helicity of the core sequence and the peptide termini. For most of the helices, we observed substantial unwinding involving at least 3 residues at both ends. For the unique case of histidine at positions 4 and 5, an extended N-terminal unwinding was observed up to residue 7. For further investigation regarding the onset of fraying, we employed A⁴⁵GWALP23 with ²H labels at residues 4 and 5 and found that the number of terminal residues involved in the unwinding depends on bilayer thicknesses and helps to govern the helix dynamics. The combined results enable us to compare and contrast the extent of fraying for each related helix, as reflected by the deviation of experimental ²H quadrupolar splitting magnitudes of juxta-terminal alanines A3 and A21 from those represented by an ideal helix geometry.

INTRODUCTION

Transmembrane alpha-helices constitute a maior structural motif for many biologically important integral membrane proteins including, for example, the seven-helix G-protein coupled receptors^{1, 2} and a wide variety of single-span membrane proteins³⁻⁵. The helices often terminate at or near the lipid membrane-water interface, vet the molecular interactions responsible for helix continuation, segment looping or helix termination are not well understood. Computational approaches to transmembrane helices sometimes presume an uninterrupted helical secondary structure 6-8 which is not necessarily validated. Some segments may loop naturally to join consecutive helices of a multi-helix membrane protein 9-12, while other transmembrane helices may extend beyond the membrane surface 13, 14. Well controlled experiments with appropriate model peptide-lipid systems can help to address some of the considerations for helix folding and protein-lipid interactions.

In this article we address the unwinding of helix terminals at a membrane/water interface, which we hypothesize may be a general property for many individual and bundled polypeptide helices that span lipid-bilayer membranes. As a choice of model system, we employ here the GWALP family of transmembrane peptide helices, which like the parent WALP peptides¹⁵ have proven useful for elucidating fundamental principles. In particular, a second-generation peptide acetyl-GGALW(LA)6LWLAGA-amide, GWALP23. exhibits favorable properties, including a well-defined tilted transmembrane orientation wherein the tilt of the GWALP23 helix scales with the bilayer thickness¹⁷. The helix furthermore undergoes only modest dynamic averaging about a principal transmembrane orientation 18, 19. Interestingly, the presence of more than two interfacial Trp or Tyr residues, flanking the central helix, tends to increase dramatically the extent of the motional averaging 18-20.

Comparisons among several derivatives of GWALP23, namely similar transmembrane helices with different numbers or locations of interfacial Trp, Tyr or Phe residues21, 22, have suggested that factors other than interfacial aromatic residues might help to determine particular orientations for neutral transmembrane helices. Experiments with deuterium labels on residues A3 and A21, separated by 18 residues or five turns on a "perfect" Thelix 23, revealed the fraving of helix terminals for acetyl-GGAAA(LA)6LWLAGA-amide GGAFF(LA)₆LWLAGA-amide in bilayer membranes²⁴ (Figure 1). Is helix fraying therefore a general feature that is commonly observed for transmembrane helices? Do particular combinations of side chains govern the location and the extent of helix unwinding? To address these questions, we have examined the influence of residues 4 and 5 for the core helix integrity and unwinding of N- and C-terminals of a series of GWALP23-like transmembrane peptides. In particular, we have compared the influence of small side chains, G⁴G⁵ and A⁴A⁵, and aromatic side chains, F⁴F⁵, Y⁴Y⁵, W⁴W⁵ and H⁴H⁵ (Table 1), for important properties such as the helix orientation, dynamic averaging and terminal fraying in bilayer membranes of DOPC, DMPC and DLPC. The results give insight into the molecular interactions of protein domains that are in direct contact with lipids in bilayer membranes.

MATERIALS AND METHODS

Peptides were synthesized on a model 433A solid-phase peptide synthesizer (Applied Biosystems) from Life Technologies (Foster City, CA) using a modified FastMocTM

chemistry on a 0.1-mmol scale, with extended times for deprotection or coupling where needed. N-fmoc amino acids were purchased from NovaBiochem (San Diego, Ca), Anaspec (Fremont, CA) and Bachem (Torrence, CA), including histidine and tryptophan whose side chains were additionally protected with trityl and t-butoxycarbonyl protecting groups, respectively. Prior to peptide synthesis, commercial L-alanine-d4, from Cambridge Isotope Laboratories was manually derivatized with an N-terminal Fmoc protecting group, as described previously 23,26, with monitoring by HNMR spectroscopy to confirm successful synthesis of FmocAla-d4. Typically, each peptide was synthesized with two deuterium-labeled alanines at 50% and 100% isotope abundance levels, to distinguish and assign the ²H NMR signals based on relative intensities.

Peptides with His-trityl and Trp-butoxycarbonyl were deprotected and cleaved from Rink amide (NovaBiochem) using a cleavage cocktail containing trifluoroacetic acid (TFA):phenol:triisopropylsilane:water in a 85:5:5:5 ratio at 22 °C for two h, to release a peptide with a neutral amidated C-terminal. After filtering the free peptide solution from resin support, peptides were precipitated with a cold 50:50 methyl-t-butyl-ether:hexane (0 °C, 30 m) mixture and collected by centrifugation. To remove traces of TFA, multiple steps of washing (with methyl-t-butyl-ether:hexane) and lyophilization (from 1:1 acetonitrile:water) were performed. Crude peptides were purified by means of reversed-phase HPLC, using a 9.4 × 250 mm Zorbax SB-C8 column packed with 3.5 µm octyl-silica (Agilent Technologies, Santa Clara, CA), eluted with a gradient of 9599% (W peptide), 88-92% (H^{4,5} peptide) or 94-98% (G^{4,5} peptide) methanol in water containing 0.1% TFA (v/v). Purified peptides were quantified by measuring the absorbance at 280 nm based on a molar extinction coefficient of 5600 M⁻¹ cm⁻ Trp⁻¹ in the peptide sequence ²⁷. MALDI-TOF analysis was used for to verify the peptide molecular mass.

Mechanically oriented samples for solid-state NMR experiments were prepared with 1:60 peptide:lipid (mol:mol) ratio, using dilauroylphosphatidylcholine (DLPC), dimyristoyl-phosphatidylcholine (DMPC) dioleoylphosphatidylcholine (DOPC) lipids (Avanti Polar Lipids, Alabaster, AL). The respective bilayer thicknesses at 50 °C (excluding the head group region) are about 20.8 Å (DLPC), 24.8 Å (DMPC) and 26 Å (DOPC) 28,29. Peptidelipid mixtures were hydrated with ²H-depleted water (Cambridge Isotope Laboratories) to achieve 45% w/w hydration following the procedure described previously 30. Solid-state NMR spectra for ³¹P nuclei (for confirming the alignment of phosphate head groups in lipid bilayers) and ²H nuclei (for analysis of peptide orientations and dynamics based on ²H-labeled alanines in the peptide) were recorded using a Bruker Avance 300 spectrometer (Billerica, MA).

The ^{31}P NMR spectra were recorded in a Doty 8 mm wide-line probe (Doty Scientific Inc., Columbia, SC) with broadband ^{1}H decoupling on a Bruker Avance 300 spectrometer at both $\beta=0^{\circ}$ (bilayer normal parallel to magnetic field) and $\beta=90^{\circ}$ macroscopic sample orientations. Measurements were performed at 50° C using the zgpg pulse program, a 6 μs 90° pulse, and a recycle delay time of 5 s. Before Fourier transformation, an exponential weighting function with 100 Hz line broadening was applied. The chemical shift was referenced externally to 85% phosphoric acid at 0 ppm.

The 2H NMR spectra were recorded at 50 °C with macroscopic sample orientations of $\beta=0^\circ$ and $\beta=90^\circ$. A quadrupolar echo pulse sequence was employed with full phase cycling, a pulse length of 3.2 μ s, echo delay of 105 μ s and a 120-ms recycle delay. Between 0.7 and one million free induction decays were accumulated during each 2H experiment. Fourier transformation was accomplished after applying an exponential weighting function with 100 Hz line broadening.

Circular dichorism measurements were performed on peptides incorporated into small unilamellar vesicles of lipids (1:60, peptide: lipid), obtained by ultrasonication treatment. Peptide concentrations were in 100 μ M range, determined by UV-Vis spectroscopy. Spectra were recorded in a Jasco J-1500 spectropolarimeter, using a 1 mm cell path length, 1.0 nm bandwidth, 0.1 nm slit and a 20 nm/min scan rate. Six scans typically were recorded and averaged to enhance signal to noise ratio.

Helix integrity, end fraying, orientation and dynamics were analyzed using two methods, a semi-static geometric analysis of labeled alanines ("GALA") 30 and a modified Gaussian approach ^{22, 32} for fitting the ²H NMR signals from the CβD3 groups of Ala-d4 residues. The GALA method fits a principal order parameter Szz, an average tilt magnitude τ_0 of the helix axis with respect to the bilayer normal and azimuthal rotation το about the helix axis, while maintaining an ε langle between the alanine Cα-Cβ bond vector and the helix axis fixed at 59.4° 30. The modified Gaussian approach also involves three variable parameters, an average helix tilt τ_0 , mean azimuthal rotation and rotational slippage while maintaining fixed values for Szz (principal order parameter) and [[] (helix wobble) that were held constant at 0.88 and 10°, respectively, following²². The helix integrity, or lack thereof, was assessed by observations of alanine side-chain CD3 | values that deviated from the quadrupolar wave plot for the core helix, following²⁴.

For the A^{4,5}GWALP23 helix, a full Gaussian analysis³³ was performed using eight data points, quadrupolar splittings for deuterated alanines 4, 5, 7, 9, 11, 13, 15 and 17. For this analysis, the search increments were 0-90° for \square , 0-360° for \square , 0-40° for \square and 0-120° for \square Then the best fits for each of the variables τ_0 , \square , \square and \square were determined.

RESULTS

Favored by (Leu-Ala)6 repeats, synthetic model peptides of the GWALP23 family adopt primarily transmembrane alpha-helical secondary structures within the hydrophobic region of a lipid bilayer, which may be further stabilized by two flanking tryptophan residues. In the modified peptides under consideration here, the L⁴W⁵ sequence of GWALP23 is replaced by neutral Gly or Ala, or by aromatic residues that may be neutral, polar or amphipathic, resulting in G^{4,5}, A^{4,5}, F^{4,5}, H^{4,5}, Y^{4,5} and W^{4,5}GWALP23 peptides (Table 1). After synthesizing and purifying the peptides, their molecular masses and ²H labeling patterns were confirmed by MALDITOF mass spectrometry (Figure S1 of the Supporting Information). The helicity of peptides was checked using circular dichroism (CD) spectroscopy in DLPC, DMPC and DOPC lipid bilayers. The CD spectra generally show double minima near 208 nm and 222 nm, which are characteristic features for alpha-helical structure (Figure S2 of the Supporting Information). [The situation may be complicated by the Trp residues in W^{4,5}GWALP23, for which the ratio \(\bigsigma 222/\subseteq 208\) in DOPC is about 1.1 instead of the more usual observation of about 0.9.] In the macroscopically oriented samples, the peptide-lipid mixtures are well aligned in bilayers, as indicated by the ³¹P NMR spectra for the lipid head groups in the $\square = 0^{\circ}$ and $\square =$

90° sample orientations (Figure S3 of the Supporting Information).

To evaluate the helix orientations and integrity in more detail, we recorded ²H NMR spectra of d₄-labeled alanine residues of G^{4,5}, H^{4,5} and W^{4,5}GWALP23 in DLPC, DMPC and DOPC bilayer samples. The ²H NMR spectra indicate freely moving peptides that are not aggregated in the lipid membranes. The twofold reduction in quadrupolar splitting magnitude when β = 90°, compared with $\beta = 0^{\circ}$ (Figure 2), shows that the peptides undergo rapid uniaxial reorientation around the normal to the oriented membranes 30. (By contrast, control peptides that aggregate display a Pake pattern 34 - which is not observed here.) The ${}^{2}H$ quadrupolar splitting magnitudes ($|\Delta vq|$) from methyl side chain (CD3) groups of six core alanines provide required data for estimating the preferred tilted and averaged orientations of the core transmembrane helical segments with respect to a bilayer normal in an applied magnetic field 30,35, and for comparing the global helix dynamics using semi-static and modified Gaussian methods 22.

Glycine and alanine comparisons. In the design of $\frac{16,17_{w}5}{}$

GWALP23, was presented as an "anchoring" interfacial Trp residue to help stabilize a well-defined tilted transmembrane orientation for the core helix. Nevertheless, the A45 derivative of GWALP23, without W5, also exhibits a well-defined transmembrane orientation for its core helix, with only a small extent of dynamic averaging 24. Now, having removed the #4 and #5 side chains altogether, we observe and report similar properties for G^{4,5}GWALP23 (Figure 2). Indeed, the ²H NMR spectra for the core alanines 7, 9, 11, 13, 15 and 17 are quite similar for G^{4,5}GWALP23 and A^{4,5}GWALP23 (Figure 2; Figure S4 of the Supporting Information). The maximal quadrupolar splitting magnitudes, those that eventually define the amplitudes of the quadrupolar wave plots (see below), are only slightly smaller with G4 and G5, compared to A4 and A5 (Table 2), indicating a similarly low extent of dynamic averaging. For example, $A^{4,5}$ produced wide ranges of $|\Delta v_q|$ magnitudes, from 6.5 to 23.2 kHz in DLPC, 6-21 kHz in DMPC and 0.5-18.6 in DOPC (Table 2), resulting in a relatively similar orientation and dynamics to GWALP23² For $G^{4,5}$ the $|\Delta v_q|$ values extend from 1.4-19 kHz in DLPC, 7.0-20 kHz in DMPC and 1-17 kHz in DOPC (Table 2). The scope, defined by the tilted helix, appears equivalent when the helices are in DMPC or DOPC bilayers, while in DLPC the quadrupolar splittings of G^{4,5} are slightly lower compared to A^{4,5} (Table 2).

For evaluation of the tilt angles, the observed quadrupolar splittings were subjected initially to a semi-static GALA analysis 30,33 , a technique that uses an α -helical geometry and a principal order parameter S_{zz} as an estimate for overall helix motion. Based on the 2H NMR quadrupolar splittings, this method finds the lowest RMSD values using three variables,

for F^{4,5}GWALP23 ^{22,24} than for Y^{4,5}GWALP23 ^{20,21}; see Additionally, helix dynamics were analyzed using a modified Figure 4 and Table 2. Gaussian analysis 22,32 that employs also a three-parameter fit, with variables being , and a rotational "slippage" about the helix axis. To maintain an equivalent "playing" field (with three parameters), the modified Gaussian method maintains fixed estimated values of Szz and T the helix "wobble" 22. The results and corresponding RMSD values obtained from the GALA and Gaussian analysis methods are listed in Table 3. The theoretical quadrupolar wave plots of versus the alanine C radial location, corresponding to the best fits for \square , \square and S_{zz} or \square are presented in Figure 3, overlaid with the experimental data. In general, Figure 3 indicates that the overall results for the G^{4,5}GWALP23 helix are quite similar to those for the parent GWALP23 peptide helix that has L4,W5 instead G4,G5. Remarkably, the helices with G',G'; A',A' or L',W' show analogous characteristics in each lipid bilayer membrane.

 S_{zz} , the mean helix tilt (τ_0) and azimuthal rotation (ρ_0), those

Notably, the small tilt angles observed for G^{4,5}GWALP23 in DMPC and DOPC (about 8° and 6° respectively) are nearly identical to those found previously ¹⁷ for the GWALP23 helix (Table 3). Results from the semi-static GALA method reveal, nevertheless, a distinctly smaller apparent tilt in DLPC

_G4,5

bilayers for the peptide helix, albeit with a similar azimuthal rotation angle (Figure 3). Indeed, G^{4,5}GWALP23 exhibits a helix tilt angle that appears about 10° lower than that observed for GWALP23, A^{4,5}GWALP23 or F^{4,5}GWALP23 in DLPC (Table 3). The modified Gaussian analysis shows general agreement with the semi-static results for helix orientation and dynamics (Table 3). Notably, the value of \(\subseteq \) which is a key indicator for high levels of dynamic averaging 18, 20, 32, remains modest (near 40°) in each of the DLPC, DMPC and DOPC bilayer membranes (Table 3). Importantly, the values for G^{4,5}GWALP23 are essentially indistinguishable from those for GWALP23 in each of the lipid membranes. As is typical for transmembrane helices that exhibit only moderate dynamic averaging,18 the fitted values for the helix tilt and azimuthal rotation from the GALA and Gaussian analytical methods tend to agree (Table 3).

<u>Aromatic residue comparisons.</u> In similar fashion, we compare the influence of different aromatic residues at positions 4 and 5, relating now $H^{4.5}$ and $W^{4.5}$ with previous

results for F⁴⁵GWALP23 and Y⁴⁵GWALP23. Compared to the parent GWALP23, W⁴⁵GWALP23 contains an extra tryptophan, W⁴ in place of L⁴. As the third polar aromatic residue in the sequence, W⁴ might have been expected to confer excessive dynamic averaging and a dramatic narrowing of the range of quadrupolar splittings for the deuterated core alanines, as observed previously for Y⁴⁵GWALP23 ^{20, 21}. By contrast, W⁴⁵GWALP23 displays wide ranges of quadrupolar splittings for the core alanine side chains when the helix is dispersed in lipid bilayers (3-22 kHz for DLPC, 2-18 kHz for DMPC and 1-15 kHz for DOPC). The ²H NMR spectral results (Figure 4, Figure S6 of the Supporting Information) contrast not only with those for Y⁴⁵GWALP23 but also with results for other WALP family analogues carrying four tryptophans, namely W^{23,17,18}ALP19, W^{23,21,22}ALP23 and W²⁵W^{19,22}ALP23 which show splitting

17, 30, 35-37

ranges that span less than 15 kHz in all cases. Indeed, the

results for W^{4,5}GWALP23 are more similar to

On the other hand, H^{4,5}GWALP23 is found to behave differently than W^{4,5}GWALP23, with an apparent membrane thickness dependence of the observed range of core alanine quadrupolar splittings (Table 2; Figure 4; Figure S5 of the Supporting Information). The range is quite wide (1-18 kHz) in DLPC, moderate (2.5-14.5 kHz) in DMPC and narrow (5.511 kHz) in DOPC bilayers. Interestingly, the |Δvq| values and ranges of H^{4,5}GWALP23 in DMPC and DOPC bilayer are very similar to those observed for the highly dynamic Y^{4,5}GWALP23. These results signify the possibility of H^{4,5}GWALP23 exhibiting comparably high levels of dynamic averaging to those of Y^{4,5}GWALP23 in lipid-bilayer membranes.

Indeed, when a pair of histidine residues is introduced in positions 4 and 5, keeping the single Trp residue (W¹⁹) near the C-terminus, H^{4,5}GWALP23 is found to behave quite differently from GWALP23 or G^{4,5}GWALP23. The semi-static GALA and Gaussian fits show some similarities with the orientational and motional properties of Y^{4,5}GWALP23, yet also some differences. H4,5GWALP23 indeed is seen to be highly dynamic, showing walues that range from about 57° in DLPC to 114° in DOPC (Table 3). In DOPC bilayer membranes, H45GWALP23 and Y45GWALP23 show similar properties, where each helix displays a small tilt angle ($\bigcirc \sim 6^{\circ}$) and similar mean azimuthal rotation (from -8° to 8°), with a very large rotational slippage ($\square > 70^\circ$; Table 3). The properties of H4.5GWALP23 and Y4.5GWALP23 diverge in the thinner DMPC and DLPC lipid membranes. Reflecting again the dynamic averaging, the best fits for now differ between the two helices and differ also from the observed for each in DOPC (Table 3). Interestingly, H^{4,5}GWALP23 displays the same mean azimuthal rotation in DMPC as DLPC, but Y^{4,5}GWALP23 does not. The values of are uniformly large for these two helices (Table 3). Depending on a choice of 5° or 10° for Y^{4,5}GWALP23 can be fitted with either low or high walues in DMPC (see Discussion). We note also that residue A21 of Y^{4,5}GWALP23 fits with the core helix in DMPC (see below).

Core helix divergence. As a new feature, the ${}^{2}H$ $|\Delta v_{q}|$ magnitude for deuterated A7, near the beginning of the core helix of $H^{45}GWALP23$, fails to fit the core helix backbone geometry in bilayers of DOPC, DMPC or DLPC. In these lipid membranes, therefore, the core helix of $H^{45}GWALP23$ extends only from about residue 9 to 19, resulting in a longer unwound N-terminal up to about residue 8 (Figure 5A). We will address residue 7 further below when we consider the unwinding of the N- and C-terminals. At present, this type of core helix unwinding at A7 is unique for $H^{4.5}$ as we do not observe such results for other $X^{4.5}$ analogues, including the highly dynamic $Y^{4.5}GWALP23$.

As noted above, a similar analogue, containing tryptophans at positions 4 and 5, shows very different results. W^{4,5}GWALP23, unlike the Y^{4,5} and H^{4,5} peptides, exhibits modest dynamic averaging and gives quadrupolar wave fits for tilt and azimuthal rotation similar to those for GWALP23 (Figure 5). The modified Gaussian analysis reveals low to moderate σρ values that increase only slightly with lipid bilayer thickness (Table 3). The overall trends are very similar for the W^{4,5}GWALP23 and GWALP23 helices in

5 DLPC, DMPC and DOPC bilayer membranes. It seems that W4 is tolerated equally as well as L4. (Actually, the σρ values for W^{4,5}GWALP23 are even slightly lower than for the already well oriented GWALP23 helix.) The azimuthal rotation ρ₀ for W^{4,5}GWALP23 changes by about 12° from DLPC to DMPC and 20° from DMPC to DOPC (Table 3), which is a slightly larger lipid dependence than observed for

GWALP23. Taken together, these results indicate that the helix properties remain quite similar when L4 is changed to W4 in the GWALP23 framework.

Helix terminal fraying. Additional considerations are the length and integrity of the core transmembrane helix. The data for the CD₃ groups of juxta-terminal alanines A3 and A21 serve to define the helical integrity near the peptide ends ²⁴. Occasionally, we find that residue A7 or A17 may deviate from the core helix geometry.

To test the unwinding of helix terminals, we labeled alanines 3 and 21 of the G^{45} , Y^{45} , W^{45} and H^{45} derivatives of GWALP23 with deuterium. The 2H NMR spectra for alanines 3 and 21 of these peptides are shown in Figure 6. The spectra display distinct and sharp peaks for the CD3 side chains. Typically, the $|\Delta v_q|$ magnitudes (Figure 3, Table 2) are different for residues 3 and 21, indicating unwinding of one or both helix ends 24 . Occasionally, as observed for G^{45} -and $H^{45}GWALP23$ in DLPC, residues A3 and A21 display the same $|\Delta v_q|$ value. A coincidence of $|\Delta v_q|$ values for A3 and A21 could indicate that the helix is intact from residue 3 through residue 21 or, alternatively, both residues 3 and 21 could deviate from the core helix (see below).

When the $|\Delta v_q|$ values for A3 and A21 are visualized next to the quadrupolar wave plots for the core transmembrane helix (Figure 3), it is evident that residues 3 and 21 deviate from the core $G^{45}GWALP23$ helix in each of the DLPC, DMPC and DOPC lipid membranes. The results for $G^{45}GWALP23$ are similar to those observed previously for $A^{45}GWALP23$ and $F^{45}GWALP23$ ". The closest approach of residue 3 or 21 to the $G^{45}GWALP23$ core helix involves residue A3 in DLPC, where the $|\Delta v_q|$ deviation is only 1.5 kHz (Figure 3). Residue A3 fits the GWALP23 helix in DOPC but not in DMPC or DLPC (Figure 4), while residue A21 is consistently off of both core helices in each of the lipid membranes.

Considering H^{4,5}GWALP23 and W^{4,5}GWALP23 (Figure 4), we find that residue A7 deviates from the core helix of H^{4,5}GWALP23 in all three lipid membranes, effectively shortening the core helix of H^{4,5}GWALP23. Residue A21 also deviates, so the core helix of H^{4,5}GWALP23 extends, at most, from residue 8-20 (yet is verified only between residues 9-17). Residue 3 of H^{4,5}GWALP23 does not change its orientation much when the lipid membrane is changed (Figure 5), as the A3 $|\Delta v_0|$ values are nearly identical in DLPC, DMPC and DOPC membranes (Table 2). The orientation of residue 3 of H^{4,5}GWALP23 indeed is probably dictated by peptide bond/lipid interactions without relation to any helix (since the core helix is already unraveled at residue 7). One notes that the similar $|\Delta v_q|$ values for A3 of H^{4,5}GWALP23 are fortuitously close to the core helix in DMPC, probably a coincidence. The core helix of W^{4,5}GWALP23 is intact between residues 7-17, with residues 3 and 21 unwound (Figure 5), very similar to the situation observed with F^{4,5}GWALP23 and A^{4,5}GWALP23²⁴.

Within the context of the helix dynamics and end fraying, we compare again the helix orientations based on contour plots for best-fit values of helix tilt

and azimuthal rotation (Figure 7). These contour plots confirm the conclusions from the GALA wave plots in Figures 3 and 5. One notes that the transmembrane helices with residues F4F5, W4W5 or A4A5 display a helix tilt that increases systematically when the host bilayer becomes thinner (Figure 7). These helices whose tilt angles scale with the bilayer thickness also display limited dynamic averaging (with generally < 50°; Table 3). By contrast, the helices with residues Y4Y5 or H4H5 display extensive dynamic averaging (with generally > 70°; Table 3) and an "apparent" helix tilt angle that is obscured by the dynamic averaging and therefore appears to depend little on the bilayer thickness (Figure 7). A revised analysis (Table 3), with set to 5, indicates a high value of also for Y^{4,5}GWALP23 in DMPC. Somewhat curiously, the helix G^{4,5}GWALP23 shows only modest dynamic averaging (Table

3) yet also a tilt angle that varies little with the bilayer thickness (Figure 7).

Sequence position for the onset of fraying. For the A⁴⁵GWALP23, additional ²H labels enabled us to examine more closely the N-terminal unraveling of the core helix. With the exception of H⁴⁵GWALP23, residue A7 is part of the core helix for each of the transmembrane peptides listed in Table 1. To expand the analysis, we have deuterated and investigated alanines 4 and 5 of A⁴⁵GWALP23. Our previous study on A⁴⁵GWALP23 ²⁴ suggested that this peptide, despite its lack of an aromatic or charged flanking residue N-terminal to the core helix, aligns well in the lipid bilayers with typical rapid reorientation about the bilayer normal ³⁰ yet little additional dynamic averaging.

Alanines A4 and A5 provide a particular opportunity for the use of deuterium labels to investigate the onset of helix fraying. Figure 8 shows the ²H NMR signals from A4 (50% d₄) and A5 (100% d₄) of A^{4,5}GWALP23. The respective $|\Delta v_q|$ values are listed in Table 2. Notably, the results for the onset of helix unraveling are lipid dependent for both boundaries of the core helix. When viewing the 2 H $|\Delta v_{q}|$ magnitudes of the A4 and A5 side chains alongside the quadrupolar wave plot for the core helix from the six central alanines of A^{4,5}GWALP23, one observes that A4 and A5 deviate from helix geometry in DLPC bilayers but are included with or very close to the core helix in DMPC and DOPC (Figure 9). The core helix is nevertheless longer in DOPC bilayers because, remarkably, residue A17 deviates from the core helix in DMPC! These results imply that both terminal segments of the tilted transmembrane helix of A^{4,5}GWALP23 respond to the lipid membrane thickness. The transmembrane helix is frayed from residues 1-5 in DLPC but only from residues 1-3 in DOPC or DMPC; yet the C-terminal segment is further frayed back to residue 17 in DMPC. In the other bilayers of DLPC and DOPC, the C-terminal is unraveled from at least residues 21-23, perhaps farther, with further information not available at this time.

Refining the analysis of helix dynamics. The differential fraying of the terminals of A^{4,5}GWALP23 in different bilayer membranes raised questions about the dynamics of the core helix. At the same time, the access to data points for deuterated A4 and A5 enabled a full Gaussian analysis of the dynamic averaging for the core helix (residues 4-17 or 4-16) in DOPC and DMPC, using the quadrupolar splitting magnitudes for seven or eight alanines. The best-fit preferred ranges of RMSD as functions of \square and \square (Figure 10) reveal now a much larger preferred value (72°) for and a much larger allowed range for (for the more "perfect" core helix in DOPC bilayer membranes (lowest panel of Figure 10). These results suggest a correlation for the helix of A^{4,5}GWALP23 being less frayed and showing more dynamic averaging in DOPC. The longer core helix would have shorter exposed "stakes" on the ends, which in turn could lead to more dynamic averaging.

DISCUSSION

The integrity of a transmembrane helix can relate to the primary protein structure at the membrane interface, the bilayer thickness and the dynamic properties of the helix. Cause and effect can sometimes propagate in either direction, as for example, changes to particular interfacial residues or the bilayer thickness may influence the helix fraying, which in turn could influence the dynamics of the core helix. Interactions between side chains and lipid head groups also could influence the molecular dynamics and the extent of helix unwinding. We will focus first on helix to non-helix transitions as a general feature at lipid membrane interfaces. We will then address the interplay among interfacial residues, bilayer thickness and the core helix length, boundaries, wobble and rotational dynamics.

Interfacial helix unwinding as a general feature. With now a large set of peptides from the GWALP23 family, one observes a core transmembrane helix that is tilted in lipid-bilayer membranes. Yet the helix geometry of the central core does not extend to the terminals of the 23-residue sequence. Instead, residues 3 and 21 consistently are observed to deviate from the core helix configuration. The terminal unraveling was first suggested for GWALP23 in DMPC bilayers ¹⁷ and then was observed for the single-Trp helices of F^{4,5}GWALP23 and A^{4,5}GWALP23 in bilayers of DLPC, DMPC and DOPC ²⁴. By comparison, an amphipathic 14-residue helical peptide, (KIAGKIA)2-amide, is found to unravel at its N-terminus when bound to the surface of DOPC or DMPC bilayers; yet the helix spans residues 4-14 all the way to the C-terminus ³⁸.

For each of the 23-residue membrane-spanning helices considered here, both the N-terminal and C-terminal tend to unwind from the core helix at the membrane interfaces. Occasionally, the unraveling is less extensive near the C-terminal, a result which may couple to increased rotational dynamics for the core helix.

Helix fraying and structural plasticity indeed may have functional relevance in a variety of membrane proteins. Consider, for example, NsaS, an intramembrane histidine kinase that helps *S. aureus* adapt to a variety of environmental stimuli. A marginally stable interfacial helical coiled-coil linker adopts a variety of conformations during antibiotic induced signaling. The flexibility of the linker region, similar to those in a number of signal transduction proteins, may provide soft coupling between the transmembrane and signaling domains.

Another example involves alpha-synuclein (\square S), a small highly conserved protein linked to Parkinson's disease that localizes to presynaptic vesicles. An N-terminal lipid-binding domain of \square S adopts helix or disordered conformations, depending on the membrane environment. Conversion from extended to broken helix has been proposed to enable \square S to bridge two closely apposed membranes. Similar behavior is observed in apolipoproteins with common sequence and structural features. Reorganization between membrane-bound extended and broken helices is thought to be important for normal protein function and may play a role aggregation and toxicity. N-terminal acetylation, present in native \square S, is found to decrease helix fraying and increase affinity for vesicles with physiological anionic lipid content.

Partial fraying of a membrane proximal region of gp41 may play a role in the fusion of HIV to target cell membranes. Unwinding of a transmembrane coiled-coil of a heterodimeric integrin receptor releases a constraint on the ectodomains, enabling ligand-induced conformational changes. The unwinding of a C-terminal helix could be important for regulating the function of Switch-associated protein-70 at a membrane surface. Helix unwinding may help cytoskeletal spectrin proteins to regulate cell deformation. The influenza A

matrix protein 2 may adjust its length by partially unwinding a helix and forming loop structures. These and other examples illustrate the need for better understanding of biophysical features that govern the continuity and unraveling of protein helices in lipid membranes.

<u>Influence of Positions 4 and 5 on Tilt and Dynamics</u> . Residues
4 and 5 influence the helix properties differently in different
membrane environments. The parent helix of GWALP23 with
residues L4 and W5 is moderately dynamic with modest values
of \square while adopting a tilt \square that adjusts to the lipid
thickness." Replacing L4 with W4 interestingly does not
increase the predicted \square Competing hydrogen bonding
interactions at the membrane interface sometimes result in
increased dynamic averaging about \square , much like the behavior
observed for Y ^{4,5} GWALP23 ²² and the original WALP peptides
with four interfacial Trp residues. 8 Notably, the dynamic
averaging about \square is much less extensive for W ^{4,5} GWALP23
than for Y ^{4,5} GWALP23. Y4 and Y5 individually are well
tolerated in the transmembrane environment.20, 22 The
combination of the Y4 and Y5 side chains, nevertheless, gives
rise to much more "slippage" about the helix axis (higher $\ \ \ \ \ \ \ \ \ \ \ \ \ $
than is observed with W4,5 in all three lipid membranes. (We
note also in the case of Y4,5 a trade-off between and
The modified Gaussian predicts a much higher of 124°
instead of 18° in DMPC ifis 5° instead of 10° (Table 3).
The case with H4 and H5 is intermediate. Although the helix
with H4 and H5 prefers the same \square in the two shorter lipids,
the rotational slippage indicated by $\ \ \ \ \ \ \ \ \ \ \ \ \ $
DMPC and further increases in the thicker DOPC bilayers
(Table 3). Competition for positioning with the polar head
groups is likely for the two imidazole side chains. The situation
is more straightforward when the hydrogen bonding ability is
is more straightforward when the hydrogen bonding ability is removed. F ^{4,5} GWALP23 exhibits lower dynamics and adapts to
is more straightforward when the hydrogen bonding ability is removed. F ^{4,5} GWALP23 exhibits lower dynamics and adapts to hydrophobic mismatch by modulating its tilt alone. So why are
is more straightforward when the hydrogen bonding ability is removed. F ^{4,5} GWALP23 exhibits lower dynamics and adapts to hydrophobic mismatch by modulating its tilt alone. So why are two neighboring tryptophan residues W4 and W5 also well
is more straightforward when the hydrogen bonding ability is removed. F ^{4,5} GWALP23 exhibits lower dynamics and adapts to hydrophobic mismatch by modulating its tilt alone. So why are two neighboring tryptophan residues W4 and W5 also well tolerated in all three membranes, as opposed to the
is more straightforward when the hydrogen bonding ability is removed. F ^{4,5} GWALP23 exhibits lower dynamics and adapts to hydrophobic mismatch by modulating its tilt alone. So why are two neighboring tryptophan residues W4 and W5 also well tolerated in all three membranes, as opposed to the complications with H4,5 and Y4,5? The additional motion may
is more straightforward when the hydrogen bonding ability is removed. F ^{4,5} GWALP23 exhibits lower dynamics and adapts to hydrophobic mismatch by modulating its tilt alone. So why are two neighboring tryptophan residues W4 and W5 also well tolerated in all three membranes, as opposed to the complications with H4,5 and Y4,5? The additional motion may arise from residues 4 and 5 (H or Y) competing for favorable
is more straightforward when the hydrogen bonding ability is removed. F ^{4,5} GWALP23 exhibits lower dynamics and adapts to hydrophobic mismatch by modulating its tilt alone. So why are two neighboring tryptophan residues W4 and W5 also well tolerated in all three membranes, as opposed to the complications with H4,5 and Y4,5? The additional motion may arise from residues 4 and 5 (H or Y) competing for favorable interactions with the polar head groups. The Trp side chains
is more straightforward when the hydrogen bonding ability is removed. F ^{4,5} GWALP23 exhibits lower dynamics and adapts to hydrophobic mismatch by modulating its tilt alone. So why are two neighboring tryptophan residues W4 and W5 also well tolerated in all three membranes, as opposed to the complications with H4,5 and Y4,5? The additional motion may arise from residues 4 and 5 (H or Y) competing for favorable interactions with the polar head groups. The Trp side chains alternatively may sample many complex interactions at the
is more straightforward when the hydrogen bonding ability is removed. F ^{4,5} GWALP23 exhibits lower dynamics and adapts to hydrophobic mismatch by modulating its tilt alone. So why are two neighboring tryptophan residues W4 and W5 also well tolerated in all three membranes, as opposed to the complications with H4,5 and Y4,5? The additional motion may arise from residues 4 and 5 (H or Y) competing for favorable interactions with the polar head groups. The Trp side chains alternatively may sample many complex interactions at the interface to adapt the indole ring to the hydrophobic lipid tail
is more straightforward when the hydrogen bonding ability is removed. F ^{4,5} GWALP23 exhibits lower dynamics and adapts to hydrophobic mismatch by modulating its tilt alone. So why are two neighboring tryptophan residues W4 and W5 also well tolerated in all three membranes, as opposed to the complications with H4,5 and Y4,5? The additional motion may arise from residues 4 and 5 (H or Y) competing for favorable interactions with the polar head groups. The Trp side chains alternatively may sample many complex interactions at the interface to adapt the indole ring to the hydrophobic lipid tail and polar head group environments. ^{48,50} We surmise that W4 and
is more straightforward when the hydrogen bonding ability is removed. F ^{4,5} GWALP23 exhibits lower dynamics and adapts to hydrophobic mismatch by modulating its tilt alone. So why are two neighboring tryptophan residues W4 and W5 also well tolerated in all three membranes, as opposed to the complications with H4,5 and Y4,5? The additional motion may arise from residues 4 and 5 (H or Y) competing for favorable interactions with the polar head groups. The Trp side chains alternatively may sample many complex interactions at the interface to adapt the indole ring to the hydrophobic lipid tail and polar head group environments. 48-59 We surmise that W4 and W5 may simultaneously be able to find appropriate
is more straightforward when the hydrogen bonding ability is removed. F ^{4,5} GWALP23 exhibits lower dynamics and adapts to hydrophobic mismatch by modulating its tilt alone. So why are two neighboring tryptophan residues W4 and W5 also well tolerated in all three membranes, as opposed to the complications with H4,5 and Y4,5? The additional motion may arise from residues 4 and 5 (H or Y) competing for favorable interactions with the polar head groups. The Trp side chains alternatively may sample many complex interactions at the interface to adapt the indole ring to the hydrophobic lipid tail and polar head group environments. ^{48,50} We surmise that W4 and

7 hydrogen bond formation. Such interactions would additionally explain combined interactions of these Trp residues could limit azimuthal rotation.	n the observed drop incompared to GWALP23 (Table 3), as the on of the helix.

Removing side chains L4 and W5 completely, as with G4 and G5, decreases the helix tilt in the thinnest bilayer, DLPC, by about 10° compared to helices having L4W5 or A4,5 (Table 3). The tilt of the G⁴⁵GWALP23 helix remains essentially the same in all three lipid membranes, and the core helix seems to adapt to the bilayer by changes of 10°-30° in its azimuthal rotation. The helix dynamics with G4 and G5 are roughly the same as with L4 and W5. The lower than expected dynamic averaging and the low tilt angle in DLPC could also be explained by helix unwinding, as the Gly residues likely are not part of the core helix. Exposed backbone carbonyl groups then would be able to reach out and form stable hydrogen-bonding interactions with head groups or water at the lipid interface.

Replacing the side chains of L4W5 with methyl groups of A4,5 also retains helix properties similar to those of GWALP23. The major difference is the increased dynamic averaging when the peptide helix is incorporated into the thicker DOPC bilayer. In this environment, A4 and A5 are part of a longer core helix that extends at least to residue 17; the less frayed helix structure could be more "slippery". In DLPC, the extent of dynamic averaging is low, with A4 and A5 unwound from the core helix. In DMPC, residue A17 is unwound from the core helix, and the rotational slippage is in between the values observed in DOPC and DLPC. When the core helix of A⁴⁵GWALP23 spans a shorter sequence, in similar fashion to G4,5, some of the free backbone carbonyl groups would be able to help stabilize the helix dynamics. The methyl side chains may play a further role, as the best-fit \square is lower with A4,5 than with G4,5.

Sequence and lipid dependence of the deviation of residues 3 and 21 from the core helix. Alanines 3 and 21 are separated by 18 residues and therefore would give identical 2H NMR signals in cases where both reside within a continuous "perfect" \Box helix. $^{23.24}H$ However, residues A3 and A21 do not give identical 2H quadrupolar splittings for any of the transmembrane helices (Table 1) considered here. Instead, the 2H $|\Delta vq|$ magnitude of either A3 or A21 (or both) deviates from the value predicted by the quadrupolar wave plot for the core helix in all cases (e.g., see figures 3, 5, 9). All of these transmembrane helices are partially unwound. What is the extent of the unraveling for the N-terminal and C-terminal of each helix?

We consider the deviation (in kHz) of experimental $|\Delta vq|$ of A3 and A21 from the theoretical magnitude that would fit the corresponding quadrupolar wave plot for the core helix. Then we use the 2H $|\Delta vq|$ deviations to derive corresponding side-chain theta angle (θ) deviations 30 from helix geometry for the A3 and A21 methyl groups. Figure 11 shows these histograms for $X^{4.5}$ peptides carrying N-flanking side chains with no

$$_{G}4,5_{A}4,5_{F}4,5$$

hydrogen bonding ability: , , and L^4W^5 . Histograms for comparisons of N-flanking aromatic side chains are shown in Figure S7 of the Supporting Information. We consider the trends with respect to lipid bilayer thickness and the sizes and identities of the residue 4 and 5 side chains. An interesting initial point is that $|\Delta vq|$ for A3 is higher and that of A21 lower than the predicted value (based on the core helix geometry) in nearly all cases. These features generate positive deviation of $|\Delta vq|$ for A3 and negative for A21 (Figure 11 and Figure S7). The exact reason for these consequences is unknown. Nevertheless, the trends indicate opposite directions of fraying for the two ends.

In the parent GWALP23 helix (with L⁴W³ in Figure 11), the deviation of A3 from the core helix follows the actual tilted orientation of the helix. The tilt of GWALP23 varies with the bilayer thickness, from about 23° in DLPC down to about 6° in DOPC (Table 3). Residue A3 likewise shows smaller deviation when the helix is moved from thinner to thicker lipid, with the A3 side chain ^{2}H $|\Delta vq|$ deviating about 7.4 kHz,

6.5 kHz and 0.5 kHz in DLPC, DMPC and DOPC, respectively, from theoretical values predicted by the core helix. The helix of F⁴⁵GWALP23 exhibits a similar difference between DLPC and DOPC, with a notably much higher deviation of A3 from the core helix in DMPC. But the G⁴⁵GWALP23 and A⁴⁵GWALP23 cousins, lacking aromatic residues 4 and 5, follow different scenarios. Notably, in DLPC the experimental |Δv_q| magnitude of A3 in the presence of G⁴⁵lies below the quadrupolar wave plot, giving rise to a negative deviation. The reason for this outcome is unknown, but the lower tilt of G⁴⁵GWALP23 in DLPC (Table 3), compared to other analogs, could be a factor to influence the direction of the helix unraveling. The A⁴⁵helix shows about the same extend of unwinding of residue A3 in all three lipids (Figure 11); the findings are notable since A4 and A5 deviate from helix geometry only in DLPC bilayers, but are included on the core helix in DOPC and are very close in DMPC (Figure 8).

Residue A21, in contrast to A3, shows negative deviation in all cases (Figure 11). With the exception of F⁴⁵GWALP23 in DLPC, the extent of deviation of A21 from the prediction of the core helix is essentially the same in each lipid membrane. The magnitude of the deviation of A21 in G⁴⁵GWALP23 is in all cases slightly less than for the other helices (Figure 11).

For the N-flanking aromatic side chains 4 and 5, the W4,5 helix displays low motional averaging ($\sigma\rho$ values) in all lipid environments (Table 3) and significant deviations of A3 and A21 from the predictions of the core helix (Figure S7 of the Supporting Information). The F4,5 helix also exhibits low motional averaging and, notably, the largest deviations of residue A21 from the core helix, especially in DLPC (Figure S7). By contrast, the Y4,5 helix undergoes very extensive motional averaging (Table 3) and has A21 very close to the core helix, suggesting a longer core helix toward the C-terminal in each of the lipid membranes (Figure S7). Moving

_H4,5

to other peptides, shows somewhat similar consequences, though the status of A3 is complicated by the fact that A7 already is away from the core helix (Figure 5). The highly dynamic peptides with Y^{4,5} or H^{4,5} display quite low extent of deviation at one or both ends, suggesting a longer core helix and again pointing toward a possible inverse link between helix dynamics and terminal unwinding. A "competition" between polar aromatic residues 4 and 5 for hydrogen bonds with lipid head groups also could contribute to high levels of dynamic averaging.

Seeing that the deviations of terminal residues from a core transmembrane helix may be directed by side chain identities as well as lipid thickness, we have compared the influence of large and small nonpolar side chains (Figure 11). Comparing the terminal unraveling of helices bearing G^{4,5}, A^{4,5} and F^{4,5}, the deviations of A21 and A3 from core helix geometry generally increase with the side chain size, although the trend is opposite for A3 in DOPC membranes (Figure 11). The largest deviations are seen for F^{4,5}GWALP23, with A3 deviating most from the core helix in DMPC, and A21 in DLPC (Figure 11).

A view of energetics at the interface. The results with deuterium labels on A4 and A5 (Figures 8-9) reveal possible links between helix fraying and the rotational averaging of the core helix. The transmembrane helix of A⁴⁵GWALP23 has no charged residues and only W19 as an interfacial aromatic residue. In DOPC membranes, the core helix extends farther toward the terminals than in thinner membranes, with the ²H quadrupolar splittings from A4 through A17 falling on the wave plot for the core helix (Figure 9). At the same time, and possibly as a correlation, the rotational slippage, around the axis of the core helix, is much larger in DOPC than in DMPC or DLPC (Table 3; Figure 10). We speculate that a full Gaussian analysis, if more data points were available, might reveal more dynamic averaging also for G⁴⁵GWALP23 in DOPC. The situation is more complicated for Y⁴⁵GWALP23, which is highly dynamic in each of the lipid systems. The results suggest that helix fraying to release peptide groups may be less important for the dynamics when polar side chains (Y4 and Y5) are able themselves to interact directly with lipid head groups. Considerations of helix unraveling at membrane interfaces, nevertheless, could be significant for molecular dynamics simulations and representations of membrane proteins.

In summary, our systematic experiments with closely related transmembrane model peptide helices have enabled us to address specific questions concerning lipid-protein interactions, helix integrity and dynamics. The central findings are: (i) All of the transmembrane helices considered here are tilted in the bilayer membrane and are somewhat unraveled, by at least three residues, at each membrane interface. (ii) The extent of the N-terminal unraveling depends upon the lipid bilayer thickness and the identities of juxtaterminal side chains at positions 4 and 5. The size and polarity of the #4 and #5 side chains help to determine the length of the core helix and the onset of helix unwinding. (iii) The extent of the C-terminal unraveling has yet to be examined. (iv) In some cases (with more examples needed), the dynamic averaging of the transmembrane helix orientation may couple to the extent of helix fraying and to the bilayer thickness. It would be of interest also to examine the helix properties when the lipid head-group [average] charge is varied in mixed lipid populations. Some of these properties will be important for the plasticity and functioning of membrane proteins.

ASSOCIATED CONTENT

Supporting Information. Supplemental figures S1 to S7, including mass spectra, circular dichroism spectra and NMR spectra. This material is available free of charge via the Internet at http://pubs.acs.org.

AUTHOR INFORMATION

Corresponding Author

*Roger E. Koeppe II, Tel. (479) 575-4976; Fax. (479) 575-4049; E-Mail: rk2@uark.edu.

Author Contributions

The manuscript was written through contributions of all authors. All authors have given approval to the final version of the manuscript.

Funding Sources

This work was supported in part by NSF MCB grant 1713242, and by the Arkansas Biosciences Institute. The peptide, NMR and mass spectrometry facilities were supported in part by NIH grant GM103429.

Notes

ACKNOWLEDGMENTS

We thank Ashley Martfeld and Venkatesan Rajagopalan for helpful discussions.

ABBREVIATIONS

DLPC, dilauroylphosphatidylcholine; DMPC, dimyristoylphosphatidylcholine; DOPC, dioleoylphosphatidylcholine; MALDI-TOF, matrix-assisted laser desorption – time of flight; TFA, trifluoroacetic acid.

REFERENCES

- [1] Hilger, D., Masureel, M., and Kobilka, B. K. (2018) Structure and dynamics of GPCR signaling complexes, Nat. Struct. Mol. Biol. 25, 4-12.
- [2] Vass, M., Kooistra, A. J., Yang, D., Stevens, R. C., Wang, M.-W., and de Graaf, C. (2018) Chemical diversity in the G protein-coupled receptor superfamily, *Trends Pharmacol. Sci.* 39, 494

512.

- [3] Landolt-Marticorena, C., Williams, K. A., Deber, C. M., and Reithmeier, R. A. (1993) Non-random distribution of amino acids in the transmembrane segments of human type I single span membrane proteins, *J. Mol. Biol.* 229, 602-608.
- [4] Arkin, I. T., and Brunger, A. T. (1998) Statistical analysis of predicted transmembrane alpha-helices, *Biochim. Biophys. Acta, Protein Struct. Mol. Enzymol.* 1429, 113-128.
- [5] Ulmschneider, M. B., and Sansom, M. S. P. (2001) Amino acid distributions in integral membrane protein structures, *Biochim. Biophys. Acta, Biomembr.* 1512, 1-14.
- [6] Reddy, T., Manrique, S., Buyan, A., Hall, B. A., Chetwynd, A., and Sansom, M. S. P. (2014) Primary and secondary dimer interfaces of the fibroblast growth factor receptor 3 transmembrane domain: Characterization via multiscale molecular dynamics simulations, *Biochemistry* 53, 323-332.
- [7] Bhate, M. P., Lemmin, T., Kuenze, G., Mensa, B., Ganguly, S., Peters, J. M., Schmidt, N., Pelton, J. G., Gross, C. A., Meiler, J., and DeGrado, W. F. (2018) Structure and function of the transmembrane domain of NsaS, an antibiotic sensing histidine kinase in *Staphylococcus aureus*, *J. Am. Chem. Soc. 140*, 74717485.
- [8] Brown, M. C., Abdine, A., Chavez, J., Schaffner, A., Torres-Arancivia, C., Lada, B., JiJi, R. D., Osman, R., Cooley, J. W., and Ubarretxena-Belandia, I. (2018) Unwinding of the substrate transmembrane helix in intramembrane proteolysis, *Biophys. J.* 114, 1579-1589.
- [9] Bischoff, L., Wickles, S., Berninghausen, O., van der Sluis, E. O., and Beckmann, R. (2014) Visualization of a polytopic membrane protein during SecY-mediated membrane insertion. *Nat. Commun.* 5, 4103.
- [10] Nikiforovich, G. V., and Baranski, T. J. (2012) Structural mechanisms of constitutive activation in the C5a receptors with mutations in the extracellular loops: Molecular modeling study, *Proteins* 80, 71-80.

- [11] Abrol, R., Kim, S.-K., Bray, J. K., Griffith, A. R., and Goddard.
 - W. A. (2011) Characterizing and predicting the functional and conformational diversity of seven-transmembrane proteins, *Methods* 55, 405-414.
- [12] Yeagle, P. L., Salloum, A., Chopra, A., Bhawsar, N., Ali, L., Kuzmanovski, G., Alderfer, J. L., and Albert, A. D. (2000) Structures of the intradiskal loops and amino terminus of the G-protein receptor, rhodopsin, J. Pept. Res. 55, 455-465.
- [13] Bennett, J. S. (2005) Structure and function of the platelet integrin αIIbβ3, J. Clin. Invest. 115, 3363-3369.
- [14] Ma, Y. Q., Qin, J., and Plow, E. F. (2007) Platelet integrin αiibβ3: Activation mechanisms, *J. Thromb. Haemost.* 5, 13451352.
- [15] Killian, J. A., Salemink, I., De Planque, M. R., Lindblom, G., Koeppe, R. E., II, and Greathouse, D. V. (1996) Induction of non-bilayer structures in diacylphosphatidylcholine model membranes by transmembrane ☐helical peptides. Importance of hydrophobic mismatch and proposed role of tryptophans., *Biochemistry* 35, 1037-1045.
- [16] Vostrikov, V. V., Grant, C. V., Daily, A. E., Opella, S. J., and Koeppe, R. E., II. (2008) Comparison of "Polarization Inversion with Spin Exchange at Magic Angle" and "Geometric Analysis of Labeled Alanines" methods for transmembrane helix alignment, J. Am. Chem. Soc. 130, 12584-12585.
- [17] Vostrikov, V. V., Daily, A. E., Greathouse, D. V., and Koeppe, R. E., II. (2010) Charged or aromatic anchor residue dependence of transmembrane peptide tilt, *J. Biol. Chem.* 285, 31723-31730.
- [18] Vostrikov, V. V., Grant, C. V., Opella, S. J., and Koeppe, R. E., II. (2011) On the combined analysis of ²H and ¹⁵N/¹H solid-state NMR data for determination of transmembrane peptide orientation and dynamics, *Biophys. J. 101*, 2939-2947.
- [19] Grage, S. L., Strandberg, E., Wadhwani, P., Esteban-Martin, S., Salgado, J., and Ulrich, A. S. (2012) Comparative analysis of the orientation of transmembrane peptides using solid-state ²H and ¹⁵N NMR: Mobility matters, *Eur. Biophys. J. 41*, 475-482.
- [20] Gleason, N. J., Vostrikov, V. V., Greathouse, D. V., Grant, C. V., Opella, S. J., and Koeppe, R. E., II. (2012) Tyrosine replacing tryptophan as an anchor in GWALP peptides, *Biochemistry* 51, 2044-2053.
- [21] Gleason, N. J., Greathouse, D. V., Grant, C. V., Opella, S. J., and Koeppe, R. E., II. (2013) Single tryptophan and tyrosine comparisons in the N-terminal and C-terminal interface regions of transmembrane GWALP peptides, *J. Phys. Chem. B* 117, 13786-13794.
- [22] Sparks, K. A., Gleason, N. J., Gist, R., Langston, R., Greathouse, D. V., and Koeppe, R. E., II. (2014) Comparisons of interfacial Phe, Tyr, and Trp residues as determinants of orientation and dynamics for GWALP transmembrane peptides, *Biochemistry* 53, 3637-3645.
- [23] Pauling, L., Corey, R. B., and Branson, H. R. (1951) The structure of proteins: Two hydrogen-bonded helical configurations of the polypeptide chain, *Proc. Natl. Acad. Sci.* U. S. A. 37, 205-211.
- [24] Mortazavi, A., Rajagopalan, V., Sparks, K. A., Greathouse, D. V., and Koeppe, R. E., II. (2016) Juxta-terminal helix unwinding as a stabilizing factor to modulate the dynamics of transmembrane helices, *ChemBioChem 17*, 462-465.
- [25] Kortenaar, P. B. W., Dijk, B. G., Peeters, J. M., Raagen, B. J., Adams, P. J., and Tesser, G. I. (1986) Rapid and efficient method for the preparation of Fmoc-amino acids starting from 9-fluorenylmethanol, *Int. J. Pept. Prot. Res.* 27, 398-400.
- [26] Greathouse, D. V., Koeppe, R. E., II, Providence, L. L., Shobana, S., and Andersen, O. S. (1999) Design and characterization of gramicidin channels, *Methods Enzymol.* 294, 525-550.
- [27] Pace, C. N., Vajdos, F., Fee, L., Grimsley, G., and Gray, T. (1995) How to measure and predict the molar absorption coefficient of a protein, *Protein Sci 4*, 2411-2423.
- [28] Pan, J., Tristram-Nagle, S., Kucerka, N., and Nagle, J. F. (2008)
 Temperature dependence of structure, bending rigidity, and bilayer interactions of dioleoylphosphatidylcholine bilayers, *Biophys. J. 94*, 117-124.
 [29] Kucerka, N., Nieh, M. P., and Katsaras, J. (2011) Fluid phase lipid areas and bilayer thicknesses of commonly used

phosphatidylcholines as a function of temperature, Biochim.

- Biophys. Acta, Biomembr. 1808, 2761-2771.
- [30] van der Wel, P. C. A., Strandberg, E., Killian, J. A., and Koeppe, R. E., II. (2002) Geometry and intrinsic tilt of a tryptophan-anchored transmembrane alpha-helix determined by ²H NMR, *Biophys. J. 83*, 1479-1488.
- [31] Davis, J. H., Jeffrey, K. R., Valic, M. I., Bloom, M., and Higgs, T. P. (1976) Quadrupolar echo deuteron magnetic resonance spectroscopy in ordered hydrocarbon chains, *Chem. Phys. Lett.* 42, 390-394.
 - [32] Strandberg, E., Esteban-Martin, S., Ulrich, A. S., and Salgado, J. (2012) Hydrophobic mismatch of mobile transmembrane helices: Merging theory and experiments, *Biochim. Biophys. Acta. 1818*, 1242-1249.
 - [33] Strandberg, E., Esteban-Martín, S., Salgado, J., and Ulrich, A. S. (2009) Orientation and dynamics of peptides in membranes calculated from ²H-NMR data, *Biophys. J. 96*, 3223-3232
- [34] Rankenberg, J. M., Vostrikov, V. V., Greathouse, D. V., Grant, C. V., Opella, S. J., and Koeppe, R. E., II. (2012) Properties of membrane-incorporated WALP peptides that are anchored on only one end, *Biochemistry* 51, 10066-10074.
- [35] Strandberg, E., Özdirekcan, S., Rijkers, D. T. S., van der Wel, P. C. A., Koeppe, R. E., II, Liskamp, R. M. J., and Killian, J. A. (2004) Tilt angles of transmembrane model peptides in oriented and non-oriented lipid bilayers as determined by ²H solid-state NMR, *Biophys. J. 86*, 3709-3721.
 - [36] Özdirekcan, S., Etchebest, C., Killian, J. A., and Fuchs, P. F. J. (2007) On the orientation of a designed transmembrane peptide: Toward the right tilt angle?, *J. Am. Chem. Soc.* 129, 1517415181.
 - [37] Esteban-Martín, S., and Salgado, J. (2007) The dynamic orientation of membrane-bound peptides: Bridging simulations and experiments, *Biophys. J. 93*, 4278-4288.
 - [38] Strandberg, E., Grau-Campistany, A., Wadhwani, P., Bürck, J., Rabanal, F., and Ulrich, A. S. (2018) Helix fraying and lipid-dependent structure of a short amphipathic membrane-bound peptide revealed by solid-state NMR, *J. Phys. Chem. B* 122, 6236-6250.
 - [39] Sung, Y.-H., and Eliezer, D. (2018) Structure and dynamics of the extended-helix state of alpha-synuclein: Intrinsic lability of the linker region, *Protein Sci.* 27, 1314-1324.
 - [40] Georgieva, E. R., Ramlall, T. F., Borbat, P. P., Freed, J. H., and Eliezer, D. (2010) The lipid-binding domain of wild type and mutant α -synuclein: Compactness and interconversion between the broken and extended helix forms, *J. Biol. Chem.* 285, 28261-28274.
 - [41] Dikiy, I., and Eliezer, D. (2014) N-terminal acetylation stabilizes N-terminal helicity in lipid- and micelle-bound α-synuclein and increases its affinity for physiological membranes, *J. Biol. Chem.* 289, 3652-3665.
 - [42] Louis, J. M., Baber, J. L., Ghirlando, R., Aniana, A., Bax, A., and Roche, J. (2016) Insights into the conformation of the membrane proximal regions critical to the trimerization of the HIV-1 gp41 ectodomain bound to dodecyl phosphocholine micelles, *PLoS ONE 11*, e0160597.
- [43] Yang, J., Ma, Y.-Q., Page, R. C., Misra, S., Plow, E. F., and Qin, J. (2009) Structure of an integrin αiibβ3 transmembrane-cytoplasmic heterocomplex provides insight into integrin activation, *Proc. Natl. Acad. Sci. U. S. A. 106*, 17729-17734.
 [44] Tokuda, N., Kawai, K., Lee, Y.-H., Ikegami, T., Yamaguchi, S., Yagisawa, H., Fukui, Y., and Tuzi, S. (2012) Membrane-induced alteration of the secondary structure in the SWAP-70 pleckstrin homology domain, *J. Biochem. 151*, 391-401.
 - [45] Takahashi, H., Rico, F., Chipot, C., and Scheuring, S. (2018) αhelix unwinding as force buffer in spectrins, *ACS Nano* 12, 2719-2727.
- [46] Liu, Y., Tan, J., Zhang, J., Li, C., Luo, Y., and Ye, S. (2018) Influenza A M2 transmembrane domain tunes its conformational heterogeneity and structural plasticity in the

lipid bilayer by forming loop structures, ChemComm 54, 59035906.

- [47] McKay, M. J., Martfeld, A. N., De Angelis, A. A., Opella, S. J., Greathouse, D. V., and Koeppe, R. E., II (2018) Control of transmembrane helix dynamics by interfacial tryptophan residues, *Biophys. J.* 114, 2617-2629.
- [48] Yau, W.-M., Wimley, W. C., Gawrisch, K., and White, S. H. (1998) The preference of tryptophan for membrane interfaces, *Biochemistry 37*, 14713-14718.
- [49] de Planque, M. R. R., Bonev, B. B., Demmers, J. A. A., Greathouse, D. V., Koeppe, R. E., II, Separovic, F., Watts, A., and Killian, J. A. (2003) Interfacial anchor properties of tryptophan residues in transmembrane peptides can dominate over hydrophobic matching effects in peptide-lipid interactions, *Biochemistry* 42, 5341-5348.
- [50] Sun, H., Greathouse, D. V., Andersen, O. S., and Koeppe, R. E., II (2008) The preference of tryptophan for membrane interfaces: Insights from N-methylation of tryptophans in gramicidin channels, *J. Biol. Chem. 283*, 22233-22243.
- [51] DeLano, W. L. (2002) The pymol molecular graphics system, Delano Scientific, San Carlos, CA.

FIGURE LEGENDS.

Figure 1. Model to illustrate unwinding of peptide terminals for the helix of H^{4.5}GWALP23, showing the observed tilt and azimuthal rotation of the core helix in DLPC bilayers. The locations of Trp19 and residues 4 and 5 are illustrated on a ribbon helix, drawn using PyMOL³¹. The deuterated alanine methyl groups are shown as space filling and are colored black for core alanines (that underlie the tilt analysis) or red for the juxtaterminal alanines 3 and 21. The depicted side-chain orientations are arbitrary.

Figure 2. Deuterium NMR spectra for 2 H-labeled core alanines A7 (50% deuterated) and A17 (100%) in $G^{45}GWALP23$ and $A^{45}GWALP23$ in oriented bilayers of DLPC. Spectra for β = 90° and β = 0° sample orientations are shown. Peptide:lipid ratio, 1:60; temperature, 50 °C.

Figure 3. Quadrupolar wave analysis of tilted peptide helices in DLPC, DMPC and DOPC bilayer membranes. A. Results for G^{4.5}GWALP23. B. Results for the parent GWALP23 peptide with L4 and W5 (core alanine data points from ¹⁷). The | \(\subseteq \subseteq \) values for alanines 3 and 21 (numbered, shown as circles) generally fail to fit the helix wave plots. In some cases (i.e., GWALP in DOPC) the \(\subseteq \subseteq \) value for A3 fits on the helical wave, while that for A21 stays off the curve.

Figure 4. Deuterium NMR spectra for 2H -labeled core alanines A15 and A17 in H ${}^{45}GWALP23$ and W ${}^{45}GWALP23$; and A11 and A15 in F ${}^{45}GWALP23$ and Y ${}^{45}GWALP23$ peptides in oriented bilayers of DLPC. Spectra for $\beta=90^{\circ}$ and $\beta=0^{\circ}$ sample orientations are shown. Peptide:lipid ratio, 1:60; temperature, 50 °C.

Figure 5. Quadrupolar wave analysis of H^{4,5}GWALP23 (A), W^{4,5}GWALP23 (B) and Y^{4,5}GWALP23 (C) helices in DLPC (black), DMPC (red) and DOPC (blue) bilayer membranes. The | | values for alanines 3 and 21 (numbered, shown as circles) generally fail to fit the helix wave plots. In H^{4,5}GWALP23, A7 of the core helix (numbered) is off the curves for all three lipid membranes. suggesting extended helix unwinding at N-terminal end up to residue 7.

Figure 6. Deuterium NMR spectra for labeled A3 (50% deuterated) and A21 (100% deuterated) of $X^{4.5}GWALP23$ peptides, where X=G, Y, H and W. Spectra are shown for oriented samples in DLPC , DMPC and DOPC lipid bilayers. Peptide:lipid ratio, 1:60; temperature, 50 °C; sample orientation, $\beta=90^{\circ}$.

Figure 7. Contour plots for solutions of helix tilt \square and azimuthal rotation \square for selected X^{45} derivatives of GWALP23 in bilayers of DLPC (black), DMPC (red), and DOPC (blue). Contour levels are drawn from 0 to 3 kHz with increments of 0.6.

Figure 8. Deuterium NMR spectra for labeled alanines 4 and 5 (50% and 100% deuterated, respectively) of $A^{45}GWALP23$ in oriented bilayers of DLPC , DMPC and DOPC. Peptide:lipid ratio, 1:60; temperature, 50 °C; sample orientation, $\beta = 90^{\circ}$.

Figure 9. GALA quadrupolar wave plots for A⁴⁵GWALP23 in DLPC (black), DMPC (red), and DOPC (blue) bilayer membranes. The | values are shown as triangles for d4-labeled core alanines, as squares for A4 and A5 and as circles for A3 and A21, with the color of the respective lipid bilayer. The values of alanines 3 and 21 are off of the wave plot regardless of the lipid thickness. The values of alanines 4 and 5 are off of the wave plot in DLPC, but on the wave plot for the core helix in DMPC and DOPC. Alanine 17 deviates from the wave plot in DMPC.

Figure 10. Contour plots showing preferred ranges of and and

for the A⁴⁵GWALP23 helix in bilayers of (A) DLPC, (B) DMPC and (C) DOPC. Contours for RMSD are drawn from 1.2 kHz (dark blue) to 6.0 kHz in increments of 1.2 kHz (other colors).

Figure 11. Deviation of experimental value from fitted value for juxta-terminal alanines 3 and 21 for several transmembrane peptide helices. A. Quadrupolar splitting, \square_{l} , deviation in kHz. B. Theta angle, θ , deviation in degrees. Results are shown for GWALP23 peptides having $G^{4.5}$, $A^{4.5}$, $F^{4.5}$ or the parent L^4W^5 sequence.

13

Name	Sequence			Referenc	e	
ranic	Acetyl-GGAL	W/I A I A -	Reference			
GWALP23	ALALWLAG		22			
	Acetyl-GGAG		This			
G4,5GWALP23	LALALALAI		work			
			WOIK			
A4,5GWALP23	Acetyl-GGAA			24		
	LALALALAI					
F4,5GWALP23	Acetyl-GGAF			22		
	LALALALAI					
Y4,5GWALP23	Acetyl-GGAY			20		
1 1,0 0 11 121 20	LALALALAI					
W4,5GWALP23	Acetyl-GGAV		This			
W4,3G WILDI 23	LALALALAI		work			
H4.5GWALP23	Acetyl-GGAH			This		
114,5G W AET 25	LALALALAI	WLAGA-	work			
				Deute	rated (d ₄)	alani
					wł	neel p
X4,5GWALP23	Lipid	7	9 (80)	11	13	1
(Ref.)		(240)	9 (80)	(280)	(120)	(3.
L4W5 (22, this	DLPC	26.4	25.5	26.9	14.6	20
work)c	DMPC	21.9	8.9	20.9	3.8	17
	DOPC	16.6	1.7	16.7	1.5	15
F4,5 (22, 24)	DLPC	23.7	23.5	25.7	19.6	23
	DMPC	20.3	-	20.6	-	2(
	DOPC	16.2	0.8	18.6	0.8	18
A4,5 (24, this	DLPC	23.2	19.0	23.6	11.7	18
work)d	DMPC	20.4	10.8	20.6	9.0	18
,	DOPC	15.4	4.0	18.6	5.2	16
G _{4,5} (This work)	DLPC	18.8	6.9	16.7	1.4	12

Table 2. Observed quadrupolar splitting magnitudes, $|\Delta v_q|$ in kHz, for d4-labeled alanines of $X^{45}GWALP23$ peptides in DLPC, DMPC and DOPC bilayer membranes

Sequence

Name

vame	Sequence			Reference	·								
GWALP23	Acetyl-GGAL ALALWLAG		LALAL	22									
G4,5GWALP23	Acetyl-GGAG LALALALAI			This work									
A4,5GWALP23	Acetyl-GGAA	4A5LALA	-	24									
F4,5GWALP23	Acetyl-GGAW4WsLALA- LALALALALWLAGA-amide Acetyl-GGAW4WsLALA- LALALALALWLAGA-amide W			22									
Y4,5GWALP23				20									
W4,5GWALP23				This work									
H4,5GWALP23	Acetyl-GGAH LALALALAI	I4H5LALA	-	This work									
				Deuter	Deuterated (d ₄) alanine location in sequence (helical wheel position, degrees) _b								
X4,5GWALP23 (Ref.)	Lipid	7 (240)	9 (80)	11 (280)	13 (120)	15 (320)	17 (160)	3 (200)	21 (200)	4 (300)	5 (40)		
L4W5 (22, this	DLPC	26.4	25.5	26.9	14.6	20.7	3.4	27.5	12.8	-	-		
work)c	DMPC	21.9	8.9	20.9	3.8	17.6	2.9	10.8	3.2	-	-		
,	DOPC	16.6	1.7	16.7	1.5	15.4	2.6	10.4	2.7	-	-		
F4,5 (22, 24)	DLPC	23.7	23.5	25.7	19.6	23.4	1.8	20.6	2.6	-	-		
, (, , ,	DMPC	20.3	-	20.6	-	20.6	3.8	20.4	2.0	-	-		
	DOPC	16.2	0.8	18.6	0.8	18.6	1.9	11.8	2.2	-	-		
A4,5 (24, this	DLPC	23.2	19.0	23.6	11.7	18.7	6.6	22.3	10.2	18.6	16		
work)d	DMPC	20.4	10.8	20.6	9.0	18.8	7.1	19.6	6.3	18.1	5.2		
	DOPC	15.4	4.0	18.6	5.2	16.4	0.5	14.4	1.8	18.6	2.0		
G _{4,5} (This work)	DLPC	18.8	6.9	16.7	1.4	12.6	7.2	10.9	10.9	-	-		
	DMPC	19	6.0	17.5	1.6	14.1	5.0	16.8	7.8	-	-		
	DOPC	15.5	1.5	15.6	1.2	15.3	2.4	16.8	4.6	-	-		
H _{4,5} (This work)	DLPC	17.9	1.1	13.3	3.5	9.4	9.8	11.3	11.6	-	-		
	DMPC	14.5	2.4	11.2	4.8	8.3	8.5	11.9	8.4	-	-		
	DOPC	11.1	6.5	9.1	6.1	10.1	5.6	11.4	5.4	-	-		
W4,5 (This work)	DLPC	21.5	15.0	20.7	9.4	17.4	3.3	22.7	8.4	-	-		
	DMPC	17.3	5.8	17.5	4.5	16.2	1.6	20.8	4.9	-	-		
	DOPC	12.8	0.9	14.4	1.4	14.9	1.3	20.8	2.3	-	-		
Y4,5 (20, 22, this	DLPC	11.6	0.5	6.9	4.6	6.9	11.6	19.2	11.6	-	-		
work)e	DMPC	11.7	3.2	10.7	2.8	10.7	4.4	18.2	7.7	-	-		
	DOPC	10.2	3.8	10.0	3.8	12.6	3.8	16.2	3.2	-	-		
Page 15 of Pept	ide	GAL	A fit resul			N	Modified (Gaussian re	esultsb	•	1		
³Values are li	sted in kHz fo	or the B =	0 sample	RMS		not listed	l () were	not record	led				

Reference

^bData points are grouped for alanines 7-17 of the cores helix, then juxta-terminal alanines 3 and 21 that are separated by eighteen residues (potentially five helical turns), and finally the intervening alanines 4 and 5 of A⁴⁵GWALP23. ^cThe data points for A3 and A21 in DLPC are newly reported here. ^dThe data points for A4 and A5 are newly reported here.

[°]The data points for A3 and A21 are newly reported here.

Name	Seque				Referenc	e									
GWALP23		yl-GGAL LWLAG	WLALA-I A-amide	LALAL	22										
G4,5GWALP23	Acety	yl-GGAG	4G5LALA WLAGA-		This work										
A4,5GWALP23	Acety	Acetyl-GGAA4A5LALA- LALALALALWLAGA-amide													
F4,5GWALP23	Acety	yl-GGAF ALALAL	22												
Y4,5GWALP23	Acety	yl-GGAY	4Y5LALA WLAGA-	20											
W4,5GWALP23	Acety	yl-GGAW	V4W5LAL LWLAGA-	A-	This work										
H4,5GWALP23 Acetyl-GGAH4H5LALA- LALALALALWLAGA-amide					This work										
					Deute	Deuterated (d ₄) alanine location in sequence (helical wheel position, degrees) _b									
V CWAIDS	, ,		7		1.1					21					
X4,5GWALP23 (Ref.)	5 1	Lipid	7 (240)	9 (80)	(280)	13 (120)	15 (320) 17 (160)	$\begin{pmatrix} 3 \\ (200) \end{pmatrix}$	21 (200)	(300)	5 (40)			
L4W5 (22, this	Γ	DLPC	26.4	25.5	26.9	14.6	20.7		27.5	12.8	-	-			
work)c		MPC	21.9	8.9	20.9	3.8	17.6		10.8	3.2	-	-			
,		OPC	16.6	1.7	16.7	1.5	15.4		10.4	2.7	-	-			
F4,5 (22, 24)		DLPC	23.7	23.5	25.7	19.6	23.4		20.6	2.6	-	-			
, (, ,		MPC	20.3	-	20.6	-	20.6		20.4	2.0	-	-			
		OPC	16.2	0.8	18.6	0.8	18.6		11.8	2.2	-	-			
A4,5 (24, this		DLPC	23.2	19.0	23.6	11.7	18.7		22.3	10.2	18.6	16			
work)d	D	MPC	20.4	10.8	20.6	9.0	18.8	7.1	19.6	6.3	18.1	5.2			
		OPC	15.4	4.0	18.6	5.2	16.4		14.4	1.8	18.6	2.0			
G4,5 (This work	(i)	DLPC	18.8	6.9	16.7	1.4	12.6	7.2	10.9	10.9	-	-			
	D	MPC	19	6.0	17.5	1.6	14.1	5.0	16.8	7.8	-	-			
		OPC	15.5	1.5	15.6	1.2	15.3		16.8	4.6	-	-			
H _{4,5} (This work	i) [DLPC	17.9	1.1	13.3	3.5	9.4		11.3	11.6	-	-			
		MPC	14.5	2.4	11.2	4.8	8.3		11.9	8.4	-	-			
		OPC	11.1	6.5	9.1	6.1	10.1		11.4	5.4	-	-			
W4,5 (This work	(x) [DLPC	21.5	15.0	20.7	9.4	17.4		22.7	8.4	-	-			
		MPC	17.3	5.8	17.5	4.5	16.2		20.8	4.9	-	-			
		OPC	12.8	0.9	14.4	1.4	14.9		20.8	2.3	-	-			
Y4,5 (20, 22, this		DLPC	11.6	0.5	6.9	4.6	6.9			11.6	-	-			
work)e		MPC	11.7	3.2	10.7	2.8	10.7		18.2	7.7	-	-			
		OPC	10.2	3.8	10.0	3.8	12.6		16.2	3.2	-	-			
Page 15 of P	eptide		GAL	A fit resul	lts			Modified	d Gaussian	resultsb		Ref	.		
					RM	ISD						_		σρ	σ

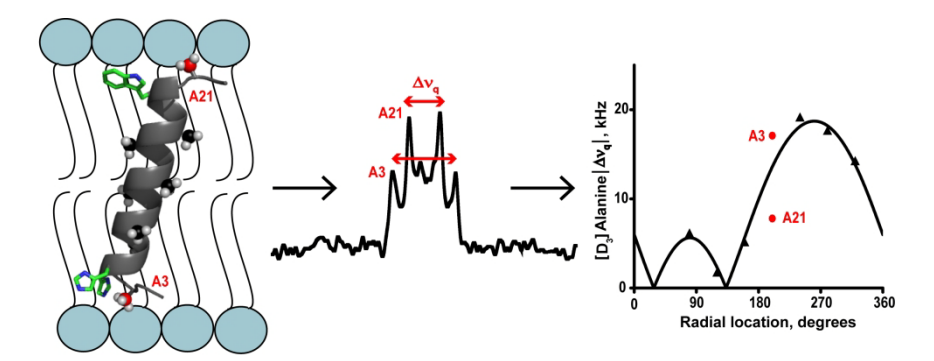
Page 15 01	1 epilde		UALA	ii iesuits		Modified	ı Gaussiaii	Kei.					
					RMSD						•	σρ	στь
of 27 Bioch		το	ρο	Szz		το	ρο						
Lipid													
DLPC	L4W5	20.7°	305°	0.66	0.71	23°	304°	33	15 _o	0.7	22		

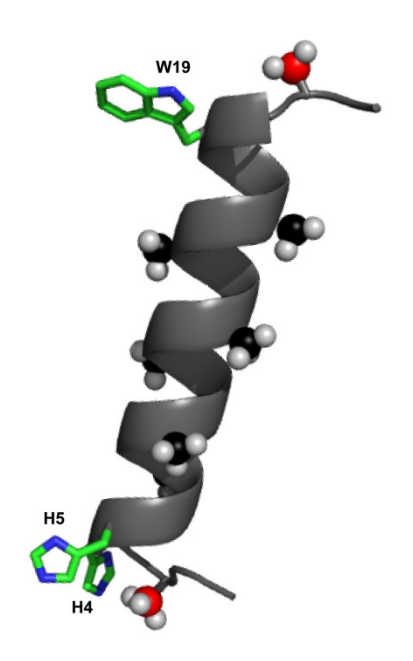
Table 3. Semi-static GALA and modified Gaussian analysis of GWALP23 and related X⁴⁵ peptide helix orientations and dynamics in bilayer membranes

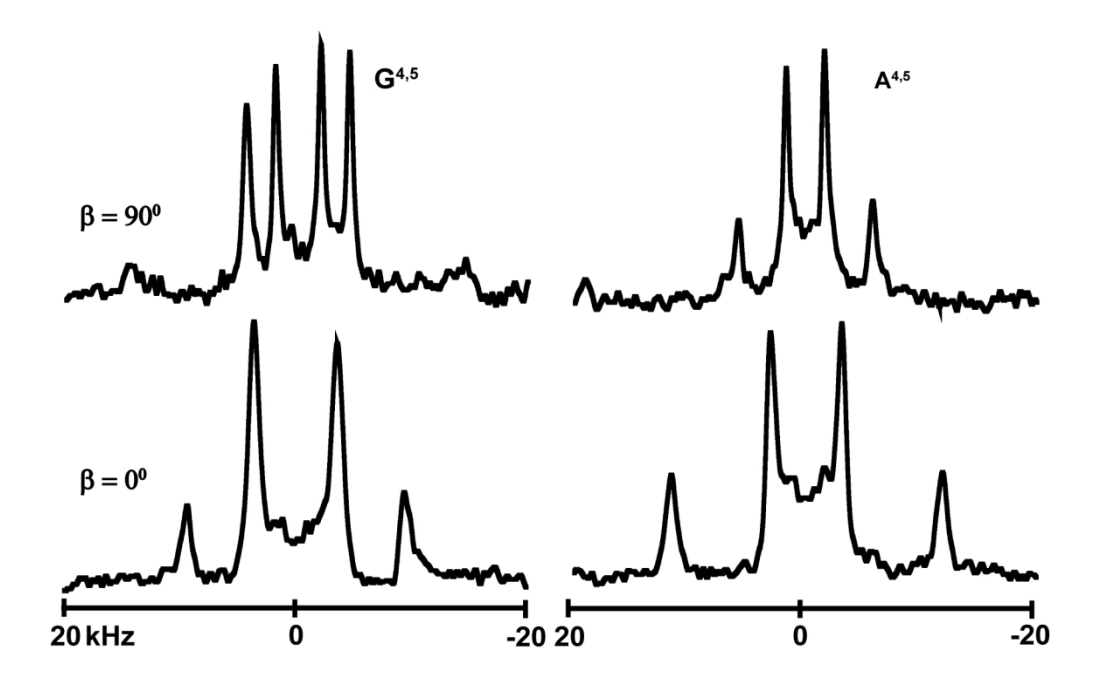
^aThe analysis methods were described previously ²². The units for RMSD are kHz. Unless otherwise noted, each analysis is based on the deuterium (²H) quadrupolar splittings for the CD3 side chains of six central alanine residues 7, 9, 11, 13, 15 and 17 in the core helix of the transmembrane peptide.

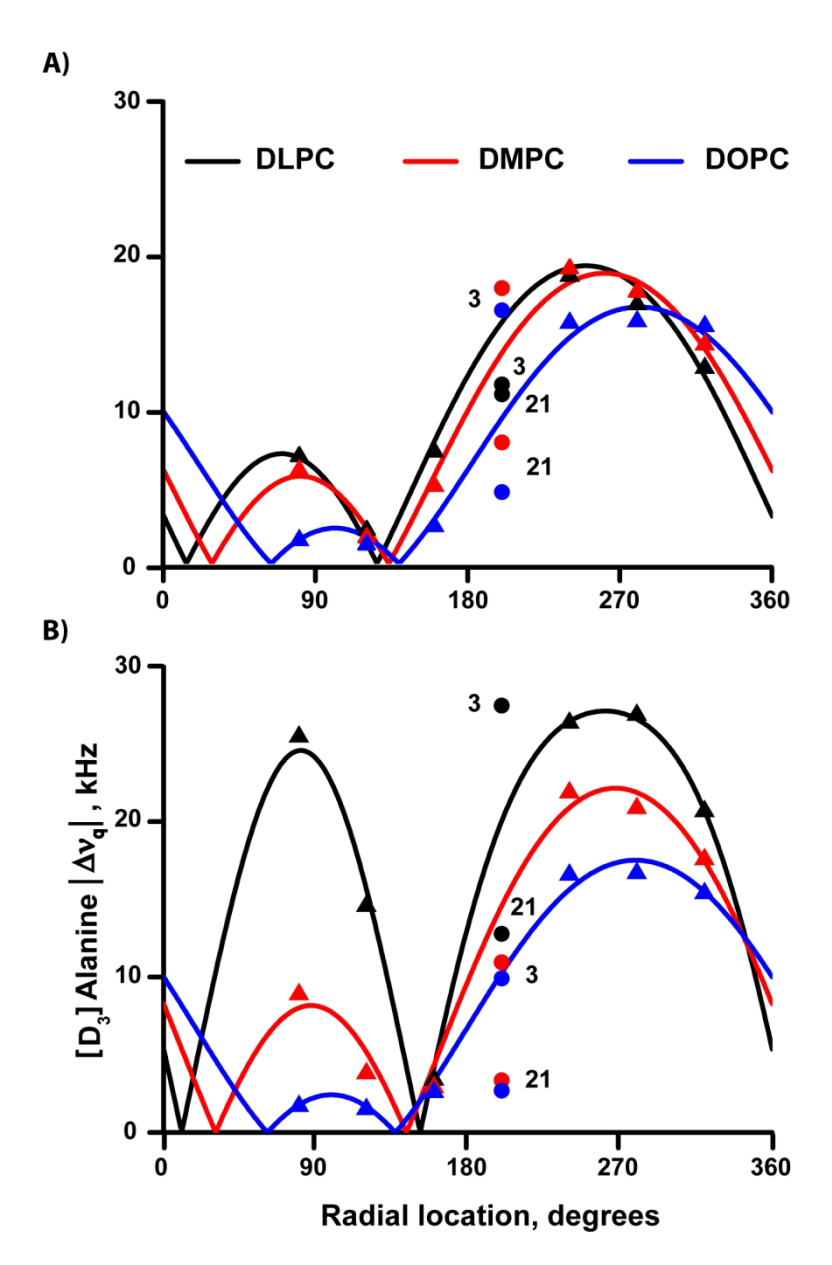
^bFor the modified Gaussian analysis ^{22,32}, was assigned the fixed value noted in the table; Szz was assigned the fixed value of 0.88. Where noted (*A^{4,5}), a GALA fit and a full Gaussian analysis (varying also were performed based on eight data points (DOPC) or seven data points (DMPC, without A17).

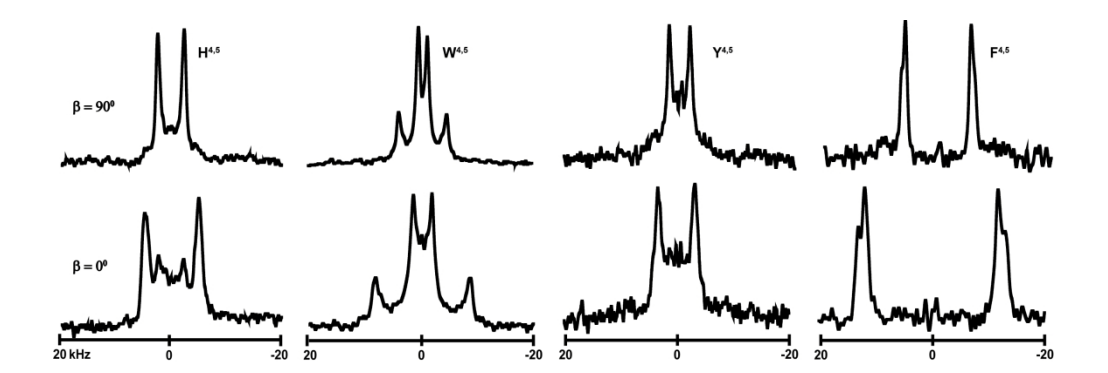
^cResidue A7 of H^{4,5}GWALP23 does not fit the quadrupolar wave plot in DMPC or DOPC and was omitted from the analysis. Curiously, residue A3 of H^{4,5}GWALP23 **does fit** the quadrupolar wave plot in DMPC (but not in DOPC). When fitting, residue A3, optionally, can be included in the analysis without altering the prediction for the helix orientation in DMPC.

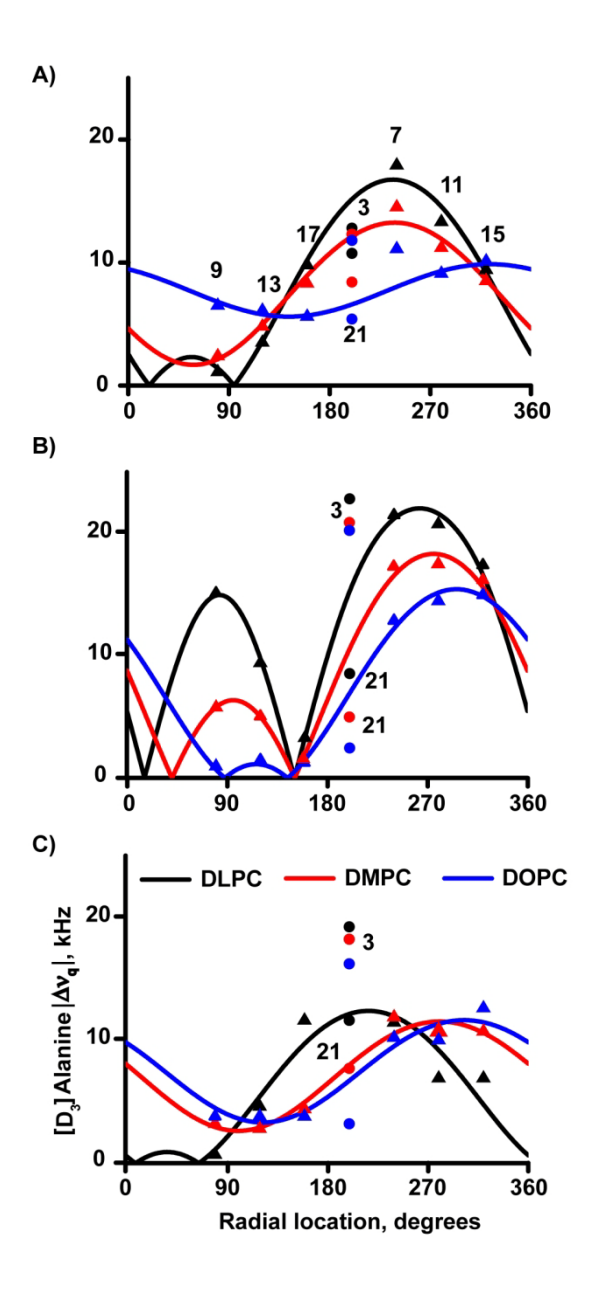


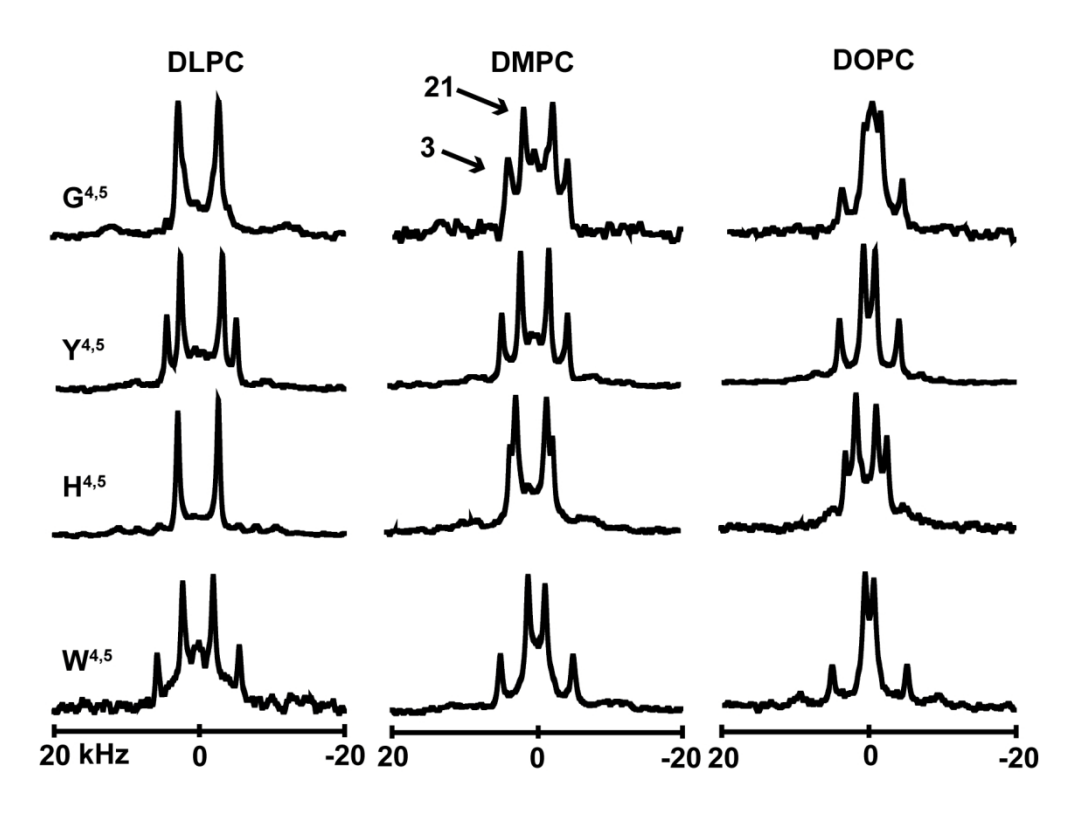




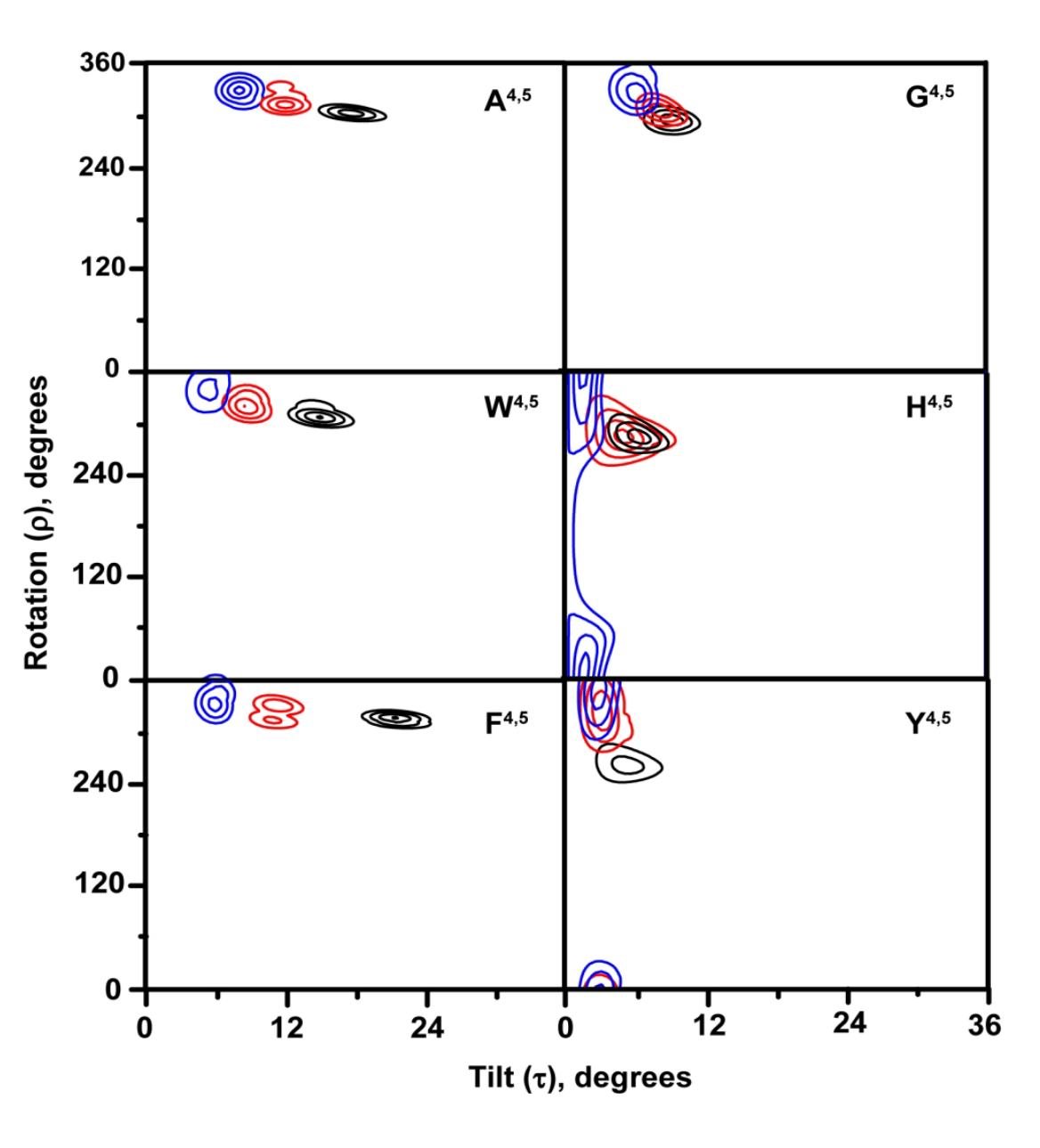


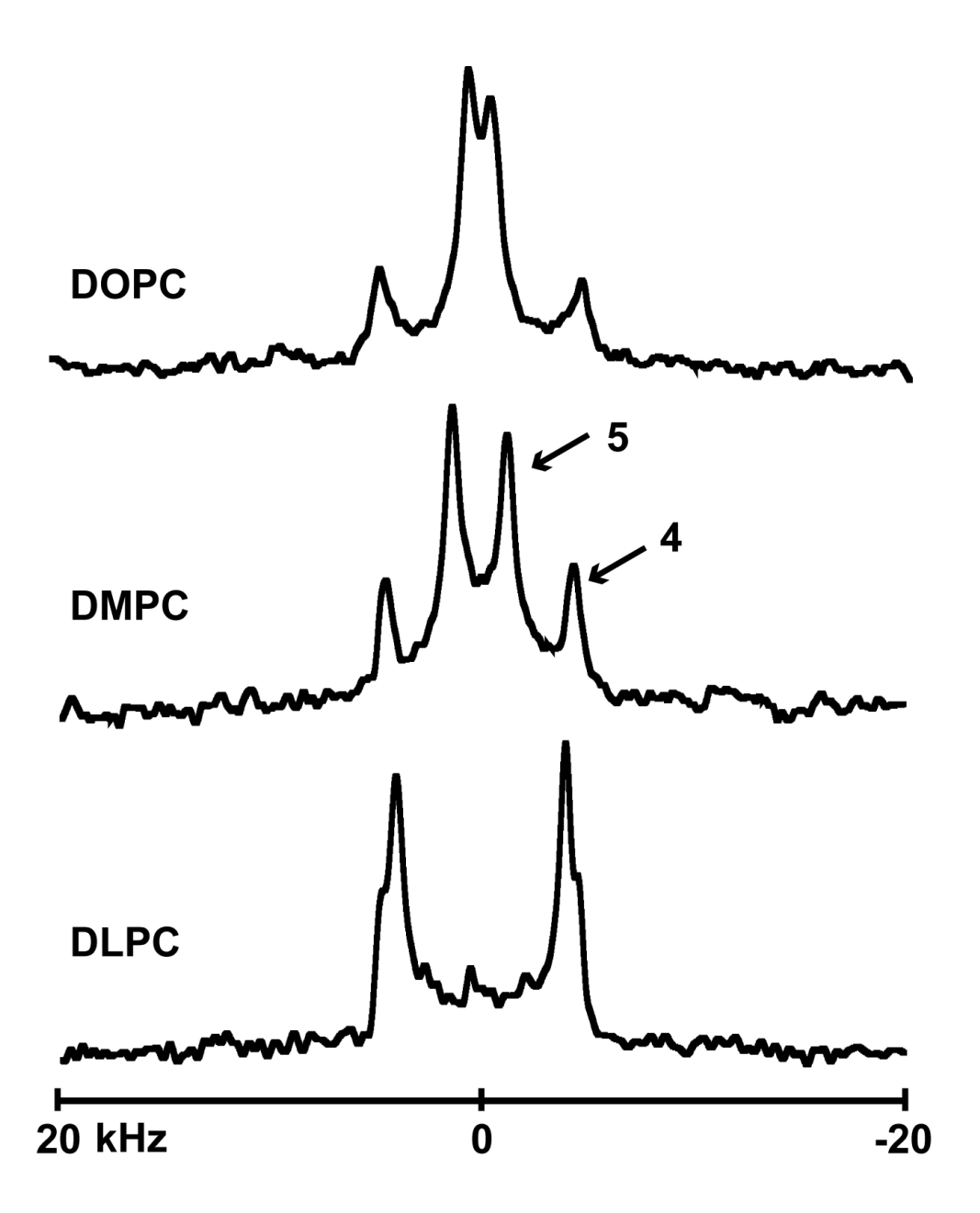


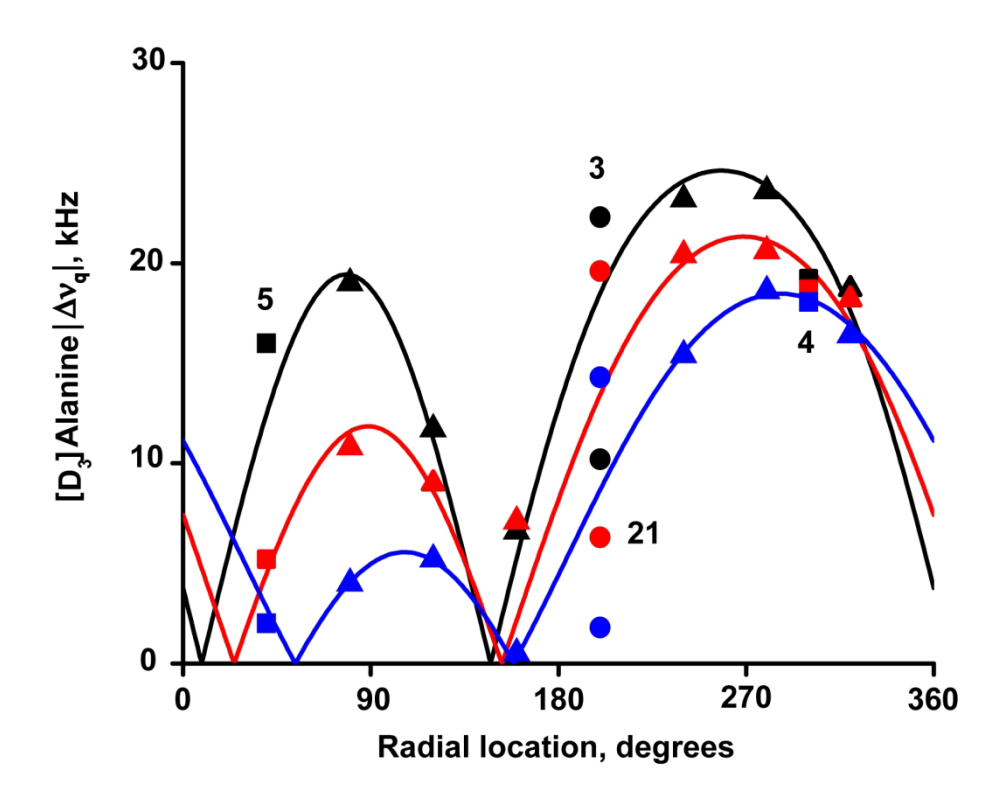


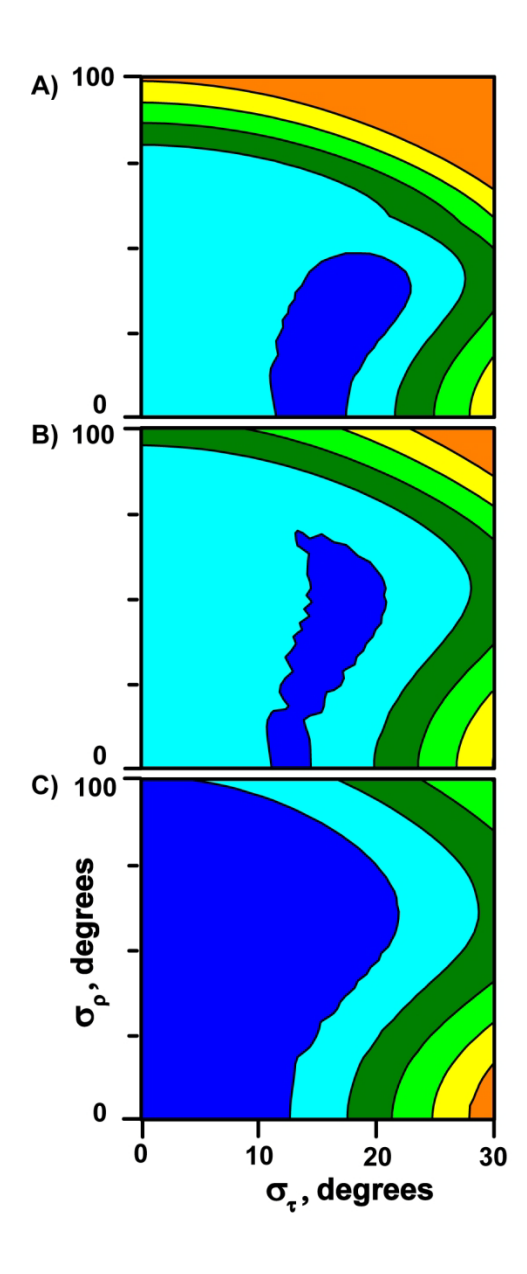


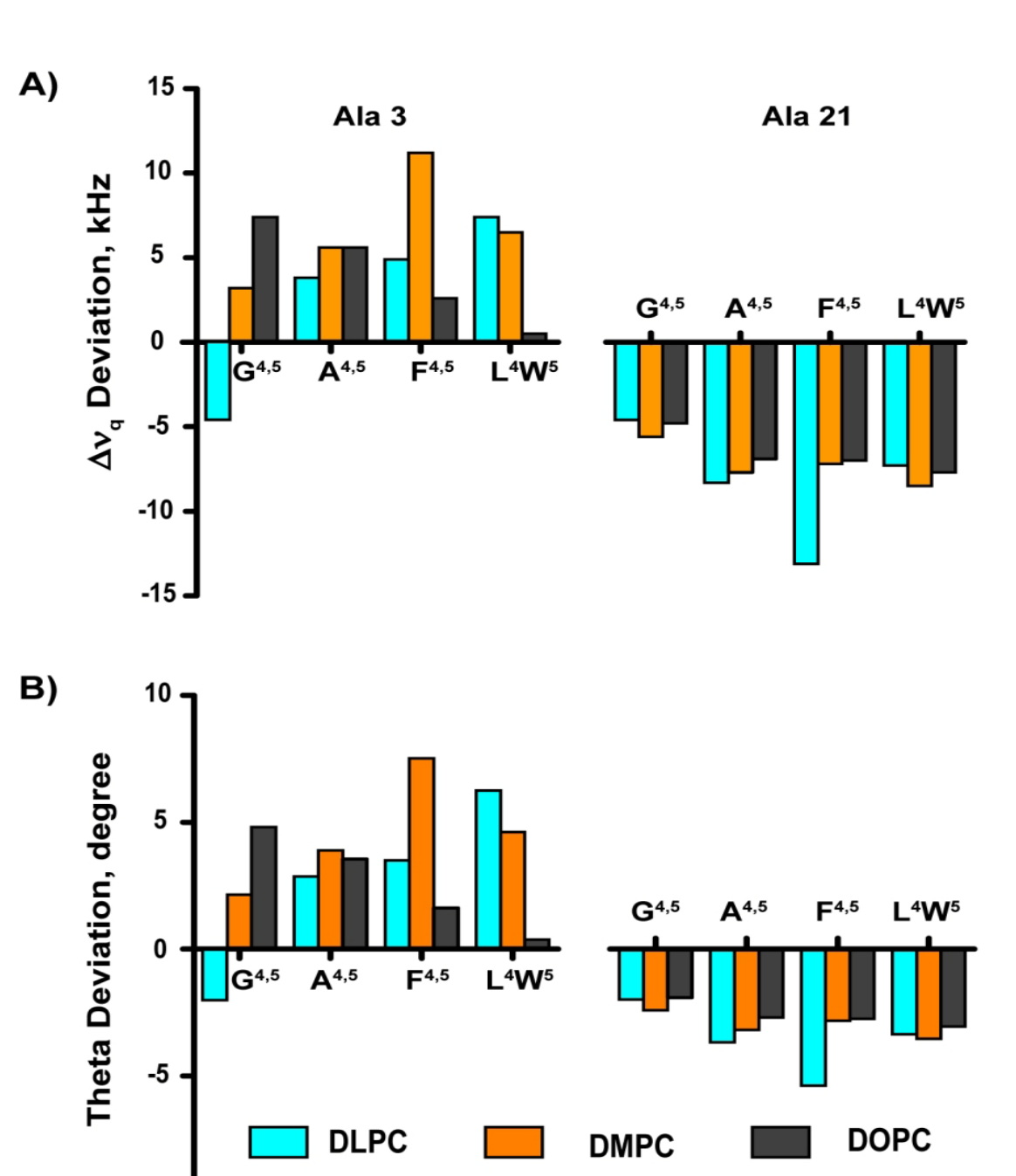
Page 23 of 27 Biochemistry











倀愀最攀......

-10

.....